Distinct stem-like cell populations facilitate functional regeneration of the *Cladonema* medusa tentacle

[1,2] Sosuke Fujita, [3] Mako Takahashi, [3] Gaku Kumano, [2] Erina Kuranaga, [1] Masayuki Miura, and [1,2,4] Yu-ichiro Nakajima*

1. Graduate School of Pharmaceutical Sciences, The University of Tokyo
2. Graduate School of Life Sciences, Tohoku University
3. Asamushi Research Center for Marine Biology, Graduate School of Life Sciences, Tohoku University
4. Frontier Research Institute for Interdisciplinary Sciences, Tohoku University

*Author for correspondence e-mail: nakaji97@g.ecc.u-tokyo.ac.jp
Tel: +81-3-5841-4863

Running title: Distinct stem-like cells enable tentacle regeneration in jellyfish
Main text: 6593 words (Abstract: 190 words)
Figures: 7
Supplementary information (Figures: 11)
Keywords: regeneration, blastema, non-bilaterians, cnidarians, jellyfish, tentacle, i-cell

Abstract

Blastema formation is a crucial process that provides a cellular source for regenerating tissues and organs. While bilaterians have diversified blastema formation methods, its mechanisms in non-bilaterians remain poorly understood. Cnidarian jellyfish, or medusae, represent early-branching metazoans that exhibit complex morphology and possess defined appendage structures highlighted by tentacles with stinging cells (nematocytes). Here we investigate the mechanisms of tentacle regeneration, using the hydrozoan jellyfish *Cladonema pacificum*. We show that proliferative cells accumulate at the tentacle amputation site and form a blastema composed of cells with stem cell morphology. Lineage tracing experiments indicate that repair-specific proliferative cells in the blastema are distinct from resident stem cells. We further demonstrate that resident stem cells control nematogenesis and tentacle elongation during both homeostasis and regeneration as homeostatic stem cells, while repair-specific proliferative cells preferentially differentiate into epithelial cells in the newly formed tentacle, analogous to lineage-restricted stem/progenitor cells observed in salamander limbs. Taken together, our findings reveal a regeneration mechanism that utilizes both resident homeostatic stem cells and repair-specific proliferative cells, which in conjunction efficiently enable functional appendage regeneration, and provide novel insight into the diversification of blastema formation across animal evolution.

Introduction

Regeneration, the phenomenon of re-forming missing body parts, is widespread among metazoans. Common regenerative processes include wound closure immediately after injury; formation of the cellular source, or blastema, that reconstitutes the lost tissue; and regrowth of the tissue that integrates different cellular behaviors such as proliferation and differentiation [1]. Among these regenerative responses, blastema formation is a critical step that can distinguish regenerative and non-regenerative systems. Indeed, most mammalian and avian species do not form blastema upon injury while wound closure normally occurs [2]. Understanding blastema formation mechanisms in highly regenerative animals may therefore help us identify the necessary elements to potentially improve our regenerative abilities.

Blastema can be defined as an undifferentiated cellular mass that contains cells with mitotic capacity and appears after damage such as amputation [3,4]. Accumulating evidence has suggested that methods of blastema formation vary among animals with high regenerative abilities [5]. For example, in planarians, pluripotent stem cells called neoblasts that are distributed throughout the body, are recruited to the injury site to produce blastema [6]. Salamanders can regenerate adult limbs upon amputation via blastema formation, but the underlying cellular mechanisms vary among species: in the axolotl, tissue-specific stem cells contribute to blastema, while in the newt, muscle fibers dedifferentiate into proliferative progenitor cells to behave as blastema [7]. During zebrafish caudal fin regeneration, both osteoblast-derived dedifferentiated cells and resident progenitor cells migrate to the wound site to form blastema [8,9]. These studies support the idea that the supply of blastema has diversified across the animal kingdom, whose members utilize resident stem/progenitor cells and/or repair-specific *de novo* proliferative cells to reconstruct lost body parts. While mechanisms of blastema formation have been extensively studied in the limited number of regenerative animals, little is known about their evolutionary characteristics: which elements are acquired as lineage-specific novelties and which are widely conserved within highly regenerative species? In particular, the current understanding of blastema formation largely relies on bilaterian models, and thus the mechanisms of blastema formation outside of bilaterians remain poorly understood.

Among various regeneration contexts, appendage regeneration is widely observed in bilaterians (e.g. amphibian limbs and fish fins), and is suitable for understanding the evolution of regenerative processes [3,10]. The bilaterian program of blastema formation during appendage regeneration is associated with repair-specific stem/progenitor cells [7,9,11]. Yet, to elucidate the evolutionary history of blastema formation programs, their mechanisms must be studied in early-branching metazoans in addition to bilaterian models.

Cnidarians (corals, sea anemones, hydroids, and jellyfish) are among the earliest branching metazoans, composed of two major groups Anthozoa and Medusozoa, forming a diverse phylum that contains over 10,000 species, and stand at a unique phylogenetic position as the sister group to bilaterians (Fig 1A). While cnidarians display considerably divergent morphologies and life cycles, represented by the polyp and medusa stages; their common traits are a diploblastic radially-symmetric body along with tentacles as the well-defined appendages that bear the stinging cells, nematocytes (cnidocytes) [12,13]. Although regenerative potential may vary among the group, most documented cnidarian species are capable of regenerating lost tissues and organs, and some can even regenerate their entire body [14,15].

Among cnidarians, polyp-type animals such as *Hydra*, *Hydractinia,* and *Nematostella* have been utilized as models to understand the mechanism of whole-body regeneration; including patterning, body axis formation, and mechanical responses [16–18]. After mid-gastric bisection in *Hydra*, cell proliferation of the stem cells, or i-cells, around the wound site is accelerated by Wnt3a produced from dying cells to generate blastema [19]. Upon decapitation of the colony polyp *Hydractinia*, i-cells remotely located in the body column migrate to the injury site to form blastema [20]. During head regeneration of the sea anemone *Nematostella*, two adult stem-like cell populations, fast-cycling cells in the body wall epithelium and slow-cycling cells in the mesenteries, migrate toward the amputation site to form blastema [21]. These studies suggest that the recruitment of resident stem cells to the injury site is a prerequisite for blastema formation after amputation of the body. However, it remains unclear whether repair-specific proliferative cells constitute the cellular source of blastema during cnidarian regeneration.

In contrast to the sessile polyp stage, medusae, commonly called jellyfish, exhibit a more complex body structure that includes multiple types of muscle such as smooth and striated muscles, developed neural networks, and

141 distinct organs and appendages, which together enable free swimming and
142 avoidance behaviors [22,23]. While most sexually-reproducing medusae do not
143 clonally propagate like polyps, medusae can still regenerate various organs and
144 appendages (e.g., manubrium, tentacle, umbrella, gonad, eye) after injury and
145 reconstitute *de novo* structures after their removal [24–30]. A recent report
146 using the hydrozoan jellyfish *Clytia* has suggested that, upon removal of the
147 entire manubrium, i-cells and differentiated cells localized in neighboring organs
148 migrate to the damage site through the canals, contributing to *de novo*
149 manubrium regeneration [27]. Despite the importance of proliferating blastema
150 cells in highly regenerative animals, the detailed mechanisms of organ and
151 appendage regeneration in medusae, particularly the mechanism of blastema
152 formation and its specific role are largely unknown.
153 The hydrozoan jellyfish *Cladonema pacificum* is an emerging jellyfish
154 model that has been utilized to study development and physiology [31–33].
155 Because *Cladonema* allows for easy lab maintenance with its high spawning
156 rate, it enables monitoring all life cycle stages and exploring organismal
157 responses to different stimuli. The genus *Cladonema* is morphologically
158 characterized by branched tentacles at the medusa stage (Fig 1B) [31,34–36].
159 The *Cladonema* medusa tentacle is primarily composed of bi-layered epithelial
160 tissues (epidermis and gastrodermis) that include muscle fiber, also called
161 epitheliomuscular cells [23]: i-cells, neurons, and nematocytes are located in the
162 epidermal layer while neurons and gland cells are located in the gastrodermal
163 layer. Resident stem cells, i-cells, are localized at the basal side of the tentacle
164 (tentacle bulb), and are thought to give rise to progenitors and differentiated
165 cells during normal development and homeostasis [24,37]. The continuous
166 growth and branching potential of the medusa tentacle makes it an attractive
167 model to understand the mechanisms of appendage morphogenesis, growth,
168 and regeneration in cnidarians.
169 In this study, we investigate the cellular mechanism of appendage
170 regeneration using the *Cladonema* medusa tentacle. Establishing the
171 *Cladonema* tentacle as an organ that can efficiently and functionally regenerate
172 upon amputation, we show that highly proliferative cells accumulate at the injury
173 site within 24 hours to behave as blastema. Lineage tracing experiments using
174 nucleoside analogs as well as dye labeling reveal that most blastema cells are
175 not derived from resident stem cells but rather appear locally after damage. We
176 further identify the role of blastema cells as the principal cellular source of the

177 epithelium in the newly formed tentacle, while resident stem cells contribute to
178 nematogenesis and tissue elongation during both homeostasis and
179 regeneration. These results suggest the existence of two distinct proliferative
180 cell populations: blastema as repair-specific proliferative cells and resident stem
181 cells as homeostatic stem cells, both of which collectively enable functional
182 tentacle regeneration. In a broader context, our findings highlight the
183 diversification of blastema formation in non-bilaterian systems, providing an
184 evolutionary insight into animal regeneration.
185
186
187 ## Materials and Methods
188
189 **Animal cultures and surgical manipulations**
190 *Cladonema pacificum* (female strain 6W) medusae were used for this research.
191 The medusae were maintained in plastic containers (V-type container, V-7, V-8,
192 and V-9; AS ONE) at 22 ℃ in artificial sea water (ASW). ASW was prepared
193 using SEA LIFE (Marin Tech) dissolved in tap water with chlorine neutralizer
194 (Coroline off; GEX Co. ltd) (24 p.p.t). The medusae were fed Vietnamese brine
195 shrimp (A&A Marine LLC).
196 Before surgical manipulation, the medusae were anesthetized with 7%
197 $MgCl_2$ in deionized water for 2 min in a petri dish (Falcon, #351008). Surgical
198 manipulations were performed with micro scissors (Teraoka, NY33408). After
199 manipulations, the medusae were quickly returned to ASW. When the tentacle
200 was amputated with the bulb left intact, the medusae were fed 1 day before
201 manipulation and were starved after amputation. When the tentacle was
202 amputated along with the bulb, the medusae were fed 1 day before
203 manipulation and were fed 3 times a week afterward.
204 Bright field pictures of medusae were taken with a LEICA S8APO
205 microscope with a Nikon digital camera (D5600) or a Zeiss AXIO Zoom.V16.
206
207 **Immunofluorescence**
208 The medusae were anesthetized with 7% $MgCl_2$ in deionized water for 5
209 min and fixed at room temperature (R.T.) for 1 h or overnight at 4 ℃ with 4%
210 paraformaldehyde (PFA) in ASW. After fixation, the samples were washed three
211 times (10 min each) with PBS containing 0.1% Triton X-100 (0.1% PBT). The
212 samples were incubated in primary antibodies in 0.1% PBT overnight at 4 ℃.

213 The antibodies used were mouse anti-acetylated tubulin (1:500; Sigma-Aldrich,
214 T6793), rabbit anti-FMRFamide (1:1000; Wako, 20091), rabbit anti-Phospho-
215 Histone H3 (Ser10) (1:500; Upstate, 06–570), mouse anti-β-catenin (8E4)
216 (1:100; Sigma-Aldrich, ALX-804-260-C100), and rabbit anti-PKC ζ C20 (1:100;
217 Santa Cruz, sc-216). After primary antibody incubation, the samples were
218 washed three times (10 min each) with 0.1% PBT. The samples were incubated
219 with secondary antibodies (1:500; ALEXA FLUOR 488, 555, 647 Goat anti-
220 mouse IgG, ALEXA FLUOR 488, 555, 647 Goat anti-rabbit IgG; Thermo Fisher
221 Scientific, A28175, A-11008) and Hoechst 33342 (1:500; Thermo Fisher
222 Scientific, H1399) in 0.1% PBT for 1 h in the dark. After three washes (10 min
223 each) in 0.1% PBT, the samples were mounted on slides with 70% glycerol.
224 Nuclear and poly-γ-glutamate were stained with DAPI (1:250; Invitrogen,
225 D1306), and actin fibers were stained with Alexa 546 phalloidin (1:400;
226 Invitrogen, A22283) in 0.1% PBT for 1 h. Confocal images were collected
227 through a Zeiss LSM 880 confocal microscope. Image processing (color
228 display) and quantification were performed using ImageJ/Fiji software.
229
230 **EdU labeling**
231 The medusae were incubated with 150 μM 5-ethynyl-2'-deoxyuridine (EdU)
232 (EdU kit; Invitrogen, C10337) in ASW for 1 h or 24 h. In chase labeling, the
233 medusae were washed with ASW at least twice (up to three times, depending
234 on amount). In pulse labeling, after EdU treatment, the medusae were
235 anesthetized with 7% $MgCl_2$ in deionized water and fixed 4% PFA in ASW. After
236 fixation, the samples were washed and incubated with a EdU reaction cocktail
237 (1× reaction buffer, $CuSO_4$, Alexa Fluor azide 488 or 647, and 1× reaction
238 buffer additive; all included in EdU kit; Invitrogen, C10337 or C10340) for 30 min
239 in the dark. After the EdU reaction, the samples were washed and incubated
240 with Hoechst 33342 in 0.1% PBT for 30 min.
241 In combination with antibody staining, EdU reaction was performed after
242 incubation with the secondary antibody. To combine EdU labeling with
243 fluorescent *in situ* hybridization (FISH), the EdU reaction was performed after
244 the incubation with Cy5-tyramide solution.
245
246 **EdU and BrdU dual labeling**
247 The medusae were incubated with 150 μM EdU in ASW for 1h or 24 h before
248 amputation, depending on the experiments. Just after incorporation of EdU, the

249 medusae were washed in ASW three times, and tentacles were amputated. At
250 24 hpa, the medusae were incubated with 2.5 mM BrdU in ASW for 1 h. The
251 medusae were washed out in ASW three times.
252 The medusae were anesthetized with 7% $MgCl_2$ for 5 min and fixed with
253 4% PFA in ASW. The samples were washed three times with 0.1% PBT and
254 incubated with a EdU reaction cocktail for 30 min in dark. The samples were
255 washed three times and treated with 2N HCl for 30 min and then washed three
256 times and incubated in primary antibodies in 0.1% PBT overnight at 4 ℃. The
257 primary antibody used was mouse anti-BrdU (1:100; BD, #347580). The
258 samples were washed three times and incubated with secondary antibodies
259 (1:500; ALEXA FLUOR 555 Goat anti-mouse IgG) and Hoechst 33342 in 0.1%
260 PBT for 1 h in the dark and washed three times.
261
262 **Fluorescent *in situ* hybridization**
263 The following FISH protocol was created from the published protocol [38]. The
264 sequences of *Nanos1, Nanos2,* and *Piwi* have been previously described [39],
265 the presumptive sequence of *Minicollagen1* (*Mcol1*) and *Vasa1* were acquired
266 from the annotation of an RNA-seq result [33]. Purified total RNA was reverse
267 transcribed into cDNA by PrimeScript II 1st strand cDNA Synthesis Kit (Takara,
268 6210A) or SMARTer™ RACE cDNA Amplification Kit (Clontech). A cDNA library
269 was used as a template for PCR (*Nanos1, Nanos2, Piwi and Mcol1*) and 3'
270 RACE (*Vasa1*). The primer sets used for PCR cloning are as follows: *Nanos1*:
271 5′-AAGAGACACAGTCATTATCAAGCGA-3′ (forward) and 5′-
272 AGCACGTAAAATTGGACACGTCG-3′ (reverse), *Nanos2*: 5′-
273 ACTTCTCCAAAACCTCATGCCGAG-3′ (forward) and 5′-
274 GAATGGCGGGCGATTTGACATCC-3′ (reverse), *Piwi*: 5′-
275 CACACAAGAGTTGGACCGGA-3′ (forward) and 5′-
276 ACCGGCTTATCGATGCAACA-3′ (reverse), *Vasa1*: 5′ -
277 GCCACCCAAAGAAGACAGACAGACAC-3′ (forward for 3′ RACE) and 5′ -
278 CGAAACGACTTGCTGATTTTCTCGCCAG -3′ (nested forward for 3′
279 RACE), *Mcol1*: 5′-CTCGTCGGTATTGCCCTCTC-3′ (forward) and 5′-
280 CCAACCTATCGTGGACGTGT-3′ (reverse). PCR products were sub-cloned
281 into the TAK101 vector (TOYOBO) and RACE product was sub-cloned into the
282 pGEM-T Easy vector (Promega). The resulting plasmids were used for RNA
283 probe synthesis with digoxigenin (DIG) labeling mix (Roche, #11277073910) or
284 fluorescein (FITC) labeling mix (Roche, 11685619910), and T7 (Roche,

285 #10881767001) or T3 RNA polymerase (Roche, #11031163001) was used,
286 according to the insert direction.
287 Medusae were anesthetized 7% $MgCl_2$ for 5 min and fixed overnight at
288 4 ℃ with 4% PFA in ASW. Briefly, fixed samples were washed three times with
289 PBS containing 0.1% Tween-20 (PBST), followed by pre-hybridization in
290 hybridization buffer (HB buffer: 5 × SSC, 50% formamide, 0.1% Tween-20, 50
291 μg/ml tRNA, 50 μg/ml heparin) at 55 ℃ for 2 h. The samples were hybridized
292 with HB Buffer containing the antisense probes (final probe concentration: 0.5–1
293 ng/μL in HB Buffer) at 55 ℃ overnight. The samples were washed twice each
294 with wash buffer 1 (5 × SSC, 50% formamide, 0.1% Tween-20), wash buffer 2
295 (2 × SSC, 50% formamide, 0.1% Tween-20), and 2 × SSC. The samples were
296 then washed with 0.1% PBST and incubated in 1% blocking buffer (1% blocking
297 reagent [Roche] in Maleic acid) for 1 h. The samples were incubated with anti-
298 DIG-POD antibodies (1:500; Roche, #11207733910) in 1% blocking buffer
299 overnight at 4 ℃. The samples were then washed with Tris-NaCl-Tween Buffer
300 and incubated with Cy5-tyramide solution (TSA Plus Cyanine 5; AKOYA
301 Biosciences, NEL745001KT) for 10 min. Finally, the samples were washed with
302 0.1% PBST and incubated with Hoechst 33342 in 0.1% PBST for 30 min in the
303 dark and washed three times.
304 For double FISH, DIG for low expression genes and FITC probes for
305 high expression genes were used (S3E Fig; *Nanos1*-DIG and *Nanos2*-FITC,
306 S3F Fig; *Mcol1*-DIG and *Nanos2*-FITC). The samples were then washed with
307 Tris-NaCl-Tween Buffer after incubation with anti-DIG-POD antibodies and
308 incubated with Cy3-tyramide solution (TSA Plus Cyanine 3; AKOYA
309 Biosciences, NEL744001KT) for 10 min. The samples were washed with 0.1%
310 PBST and incubated with 3% H_2O_2 for 15 min. The samples were washed with
311 0.1% PBST and incubated with anti-Fluorescein-POD antibodies (1:500; Roche,
312 #11426346910) in 1% blocking buffer overnight at 4 ℃. The samples were then
313 washed with Tris-NaCl-Tween Buffer and incubated with Cy5-tyramide solution
314 for 10 min. Finally, the samples were washed with 0.1% PBST and incubated
315 with Hoechst 33342 in 0.1% PBST for 30 min in the dark and washed three
316 times.
317
318 **DiI injection**
319 Medusae were relaxed in 7% $MgCl_2$ on a petri dish. 10 mM CellTracker CM-DiI
320 (Invitrogen, C7001) was injected into the epidermal layer of the tentacle bulb or

321 the center of the tentacle, using a micro injector (Eppendorf, Femtojet 4i). The
322 quartz capillary (Sutter Instrument, QF100-70-10) was pulled by Laser-Based
323 Micropipette Puller P2000 (Sutter Instrument). After injection, injected tentacles
324 were amputated. To identify DiI labeled cells, medusae were incubated with 150
325 μM EdU for 1 h before DiI injection or antibody staining was performed after DiI
326 injection using anti-β-catenin. To monitor DiI labeled cells during blastema
327 formation, at 24 hpa, the injected medusae were incubated with 150 μM EdU in
328 ASW for 1 h. The medusae were relaxed in 7% $MgCl_2$ and fixed in 4% PFA.
329 After washing in 0.1% PBT, the medusae were incubated with an EdU reaction
330 cocktail for 30 min in the dark. After the EdU reaction, the samples were
331 washed and incubated with Hoechst 33342 in 0.1% PBT.
332
333 **X-ray irradiation**
334 The medusae were placed in a V7 plastic container with 6-8 ml of ASW, the
335 minimum required for their maintenance. X-ray irradiations were performed
336 using an X-ray machine (mediXtec, MX-160Labo). Medusae were positioned 19
337 cm from the X-ray source, and a dose of 30 Gy (19.3 minutes at 160 kV 3 mA),
338 50 Gy (32.2 minutes at 160 kV 3 mA), or 75 Gy (48.3 minutes at 160 kV 3 mA)
339 was delivered. After irradiation, the medusae were moved to a plastic container
340 with fresh ASW.
341
342 **Drug treatment**
343 The medusae were incubated with 10 mM hydroxyurea (HU) (085-06653;
344 Wako, Osaka, Japan) or 30 μM Mitomycin C (139-18711; Wako, Osaka, Japan)
345 in ASW (ASW only for control). Drug incubation was sustained over 3 days.
346 Medusae were fed every other day, and the drug solutions were renewed after
347 feeding.
348
349 **qPCR**
350 Total RNA was purified from the whole tentacles of three medusae with RNeasy
351 Mini kits (Qiagen). Lysate was treated with Dnase I (Qiagen, #79254) for 15
352 min at RT. cDNA was synthesized from 200 ng of total RNA by Prime script RT
353 master Mix (Takara, RR036A). RT-qPCR was performed using TB Green
354 Premix Ex TaqII (Tli RnaseH Plus) (Takara, RR820L) and a Quantstudio6 Flex
355 Real-Time PCR system (Thermo Fisher) using *F-actin capping protein subunit*
356 *beta* as an internal control [32]. The qPCR primer sets are as follows:

357 *CpCapZbeta*: 5'-AAAGAAAGCTGGAGACGGTTCA-3' (Forward), 5'-
358 GTAGTGGGCATTTCTTCCGC-3' (Reverse), *Nanos1*: 5'-
359 TTCGTCAAGTGGCAGTCGTG-3' (Forward), 5-
360 CAAGCCCTGGTACAAACGGA-3' (Reverse).
361
362 **UV laser exposure**
363 Tentacles were amputated at 1 day before UV exposure. At 24 hpa, the
364 medusae were incubated with Hoechst 33342 (1:250) for 20 min and washed
365 three times in ASW. After washing, the relaxed medusae were placed on slides
366 with 7% $MgCl_2$ and enclosed with cover glass. UV laser was exposed to the
367 blastema region of the amputated tentacle using the photo bleaching application
368 (50 cycles at 100% 405 laser power) of the Zeiss LSM 880 confocal
369 microscope. The bleached region is shown with a white dot square (400 x 400
370 pixels, W x H) in S11B Fig. After UV exposure, the medusae were moved to
371 ASW in plastic containers and monitored to examine the effect on regeneration.
372
373 **Quantification and statistical analysis**
374 *Distribution of cells*
375 Three areas were defined (the basal, middle, and distal regions) by dividing the
376 tentacle into three equal lengths in confocal images (Figs 2A-2B, 3C-3D and
377 S2A-S2B). The number of $PH3^+$, EdU^+, or *Nanos1*$^+$ cells were counted manually
378 in each area using the multipoint tool of ImageJ/Fiji.
379
380 *Counting the number of cells*
381 The $PH3^+$, EdU^+, or *Nanos1*$^+$ cell ratio (Figs 2D-2F, 4I-4J and S7B-S7C, S7E-
382 S7F) was measured by counting the total number of cells as well as the $PH3^+$,
383 EdU^+, or *Nanos1*$^+$ cells using ImageJ/Fiji. Each signal$^+$ cell was counted
384 manually using the multipoint tool of ImageJ/Fiji. Total cell number quantification
385 was performed as follows: (1) Binarize the signal of Hoechst staining using the
386 'Threshold' command. (2) Divide continuously adjacent multiple nuclei using the
387 'Watershed' command. (3) Measure the number of nuclei using the 'Analyze
388 Particles' command.
389 Other cell number counting (Figs 3A-3B, 3E-3F, 4C-4F, 5B-5C, 5F-5G,
390 6B-6C, 6E-6F and S2C, S2E, S4C-S4E, S5A-S5D, S6B-S6C, S8A-S8B, S10,
391 S11C-S11D) was performed manually using the multipoint tool of ImageJ/Fiji.
392

393 *Measurement of tentacle length and area, signal intensity*
394 The tentacle length (Fig 5K and 6I) was measured using the segment line tool
395 of ImageJ/Fiji. The tentacle area (S5C-S5E Fig) was recorded as the ROI with
396 the polygon selection tool and measured by ImageJ/Fiji. The quantification area
397 was marked with rectangle tool, and the signal intensity was measured by
398 ImageJ/Fiji (Fig S2D).
399
400 *Statistics*
401 Statistical analyses were performed using Excel and Graphpad Prism9. Two
402 tailed *t* tests were used for comparisons between two groups. Significance is
403 indicated in the figures as follows: *P≤0.05, **P≤0.05, ***P≤0.001, Not
404 Significant (N.S.): P>0.05. Bar graphs show mean ± standard error. Dots in bar
405 graphs and boxplots indicate individual values.
406
407
408 **Results**
409 For cnidarians, tentacles are essential and common appendages for capturing
410 prey and defending against predators. Cnidarian polyps such as *Hydra*,
411 *Hydractinia*, and *Nematostella* have tentacles in the head region, near the
412 hypostome, which can restore functional tentacles during head regeneration
413 [18,20,40]. Similarly, studies using hydrozoan jellyfish have shown that
414 medusae tentacles can regenerate upon amputation [24,27]. Although
415 cnidarians commonly exhibit high regenerative capacity for tentacles, the exact
416 cellular processes and the limitation of regeneration are poorly understood.
417 To monitor the process of tentacle regeneration and to explore its
418 responses to different dissections, we utilized the medusa tentacle of the
419 hydrozoan jellyfish *Cladonema* (Fig 1). In *Cladonema* tentacles, proliferative
420 cells including stem cells, or i-cells, are localized on the basal side, called the
421 tentacle bulb, while nematocytes are distributed as clusters on the distal side,
422 similar to the jellyfish *Clytia* (Figs 1C, 2Ai, 3Ci, and S1A, S3A-S3D, S4Ai, S4Bi)
423 [24,37,39]. The existence of localized stem cells at the bulb prompted us to
424 examine tentacle regeneration as a model for appendage regeneration in non-
425 bilaterians.
426
427 ***Cladonema* medusa tentacles functionally regenerate upon amputation**

428 When the tentacle was amputated with the bulb left intact (Fig 1D and 1E),
429 wound closure finished by 24 hours post-amputation (hpa) (S1B and S1C Fig),
430 at which point the injury site became smooth surface (Fig 1Di and 1Dii).
431 Subsequently, tentacles began to elongate distally, and nematocyte clusters,
432 the spherical structures stained with the mature nematocyte marker poly-γ-
433 glutamate, formed at the tip of the regenerating tentacle at 48 hpa (Figs 1Diii,
434 1Fiii, and S1A). The number of nematocyte clusters increased during tentacle
435 elongation, and these clusters were localized along the distal side at 72 hpa,
436 which is when the regenerating tentacle branched, a characteristic feature of
437 the genus *Cladonema* (Fig 1Div and 1E). Notably, these regeneration
438 processes occurred without feeding, suggesting that tentacle regeneration is an
439 immediate response for the organism to re-construct the organ that is required
440 for capturing food.
441 To investigate the subtleties of tentacle morphology at cellular
442 resolution during regeneration, we visualized the muscle fibers, mature
443 nematocytes, and neurons by staining F-actin, poly-γ-glutamate, and
444 FMRFamide and acetylated tubulin, respectively (Figs 1F, 1G and S1D, S1E).
445 During the early stages of regeneration (0-24 hpa), wound closure occurred
446 progressively via the accumulation of supra-cellular actin fibers (Fig 1Fi and
447 1Fii). Accordingly, muscle fibers regenerated during tentacle elongation (Fig
448 1Fiii and 1Fiv). While mature nematocytes were rarely found in the bulb or the
449 injury site until 24 hpa (Fig 1Fi and 1Fii), nematocytes began to accumulate at
450 the tip of the regenerating tentacle at 48 hpa and formed clusters at 72 hpa (Fig
451 1Fiii and 1Fiv). The re-formation of neurons on the distal side occurred at 48
452 hpa and completed at 72 hpa (Figs 1G and S1D, S1E). These results suggest
453 that the regenerating tentacle is fully functional after 48 hpa. To test this
454 possibility, we examined whether the regenerating tentacle is capable of
455 feeding. While the regenerating tentacle was not functional until 24 hpa, more
456 than half of the regenerating tentacles captured prey at 48 hpa (55%), and this
457 ratio reached 100% at 72 hpa (Fig 1H and 1I). These results indicate that
458 *Cladonema* medusae can fully regenerate a functional tentacle within 2-3 days
459 of amputation.
460 While the *Cladonema* medusa tentacle can almost always regenerate
461 with the bulb left intact, it is unclear whether the tentacle can still regenerate
462 even after the bulb has been removed (Fig 1Ji). We thus ablated the entire
463 tentacle, including the bulb, and monitored the regeneration process. After

464 amputation, the ring canal and the radial canal adhered, and the wound closure
465 completed at 1 day post-amputation (dpa) (Fig 1Jii). The injured area began to
466 bulge as early as 5 dpa, and the transparent wound site turned orange, which
467 reflects the color of its food, *Artemia* (Fig 1Jiii). The *de novo* tentacle bulb
468 reformed within 1-2 weeks with a nematocyte cluster at the tip, and the small
469 tentacle gradually elongated (Fig 1Jiv and 1K). Because the rate of successful
470 regeneration varied dramatically while rearing medusae under the same
471 conditions and feeding frequency, tentacle bulb regeneration likely depends on
472 the health condition of the individual medusa (S1F Fig).
473 We also examined the regenerative potential of isolated tentacles.
474 While the whole body cannot be regrown from isolated tentacles in *Hydra* or
475 *Nematostella* [21,41], polyps in the jellyfish *Aurelia aurita* can regenerate from
476 isolated tentacles [42]. To examine the regeneration capacity of the isolated
477 tentacle in *Cladonema*, we cultured *Cladonema* medusa tentacles either with or
478 without the bulb left intact. Although wound closure successfully occurred
479 regardless of the existence of the bulb, tissues and organs located to the
480 proximal side of the tentacle including the umbrella, the radial canal, and the
481 bulb, did not regenerate, and the isolated tentacle gradually degenerated (S1G
482 and S1H Fig).
483 These observations together show that the *Cladonema* medusa tentacle can
484 functionally regenerate after amputation, but that its organ repair capacity is
485 restricted to the organism that recognizes the missing tentacle, likely through
486 the canals, as previously shown in the *Clytia* medusa [27]. For our remaining
487 studies, we focused our attention on the process of tentacle regeneration with
488 the bulb intact, which provides a highly reproducible and tractable system.
489
490 **Blastema is formed in the early phase of tentacle regeneration**
491 During organ regeneration, blastema forms at the regenerating tip after wound
492 closure and contributes to reconstruction of the new tissue as a source of cell
493 proliferation and differentiation [1,2]. In order to investigate the timing of
494 blastema formation during *Cladonema* tentacle regeneration, we performed
495 pulse labeling of EdU, a S-phase marker (Fig 2A) [43]. To understand the
496 spatial pattern of cell proliferation, we defined three areas in the regenerating
497 tentacle (the basal, middle, and distal regions) and quantified the distribution of
498 proliferating cells. Consistent with the localization of stem cells (Figs 3Ci and
499 S4Ai, S4Bi)[39], cell proliferation in the intact tentacle was mainly detected on

500 the basal side (Fig 2Ai and 2B). By contrast, cell proliferation in the regenerating
501 tentacle was frequently observed on the distal side near the wound area at 24
502 hpa (Fig 2Aii and 2B). At 72 hpa, unlike at 24 and 48 hpa, cell proliferation was
503 detected in the middle and on basal side, not on the distal side (Fig 2Aiv and
504 2B). To investigate the exact timing of the cell proliferation increase at the injury
505 site, we examined the localization of EdU^+ cells every four hours immediately
506 after amputation to 24 hpa (S2C Fig). We found that the number of proliferating
507 cells significantly increased at 20 hpa and peaked at 24 hpa (S2D-S2E Fig). We
508 further confirmed the pattern of proliferating cells using the M-phase marker,
509 anti-Phospho-Histone 3 (PH3) antibody. While $PH3^+$ cells were distributed
510 across the basal side before amputation, in the regenerating tentacle, $PH3^+$
511 cells accumulated on the distal side at 24 hpa, and gradually localized on the
512 basal side starting at 48 hpa (Figs 2D and S2A, S2B), which is consistent with
513 the results of EdU^+ cell distribution (Fig 2A and 2B). These results also reflect
514 the fact that differentiated nematocytes accumulate on the distal side at 48 hpa
515 and 72 hpa (Fig 1D and 1F). Together, these observations suggest that cell
516 proliferation is accelerated near the injury site at 24 hpa.
517 Blastema cells are undifferentiated cell populations that possess a high
518 mitotic capacity during regeneration [44]. We thus investigated proliferative
519 activity in detail during the early phase of tentacle regeneration (Fig 2D-2F). In
520 the regenerating tip, the number of $PH3^+$ and EdU^+ cells was about 4 and 20
521 times greater, respectively, than the corresponding area (amputation site) in the
522 intact tentacle (Fig 2D-2F). Moreover, these $PH3^+$ and EdU^+ cell numbers at the
523 regenerating tip were significantly greater than those in the bulb of the intact
524 tentacle where resident stem cells are localized (Fig 2D-2F). Notably, nearly
525 half of the cells in the regenerating tip are EdU^+ cells (Fig 2Dii and 2F).
526 Altogether, these results indicate that proliferative activity in the regenerating tip
527 is much higher than that of cells not in the regenerating tip, which provides
528 evidence that blastema cells appear during tentacle regeneration.
529 To determine whether blastema formation is specific to the location of
530 amputation, we examined the localization of proliferating cells after dissecting
531 tentacles in different ways. When the distal side of the tentacle is amputated,
532 ectopic cell proliferation was observed near the injury site at 24 hpa (Fig 2G).
533 Similarly, when the tentacle was amputated with the bulb, cell proliferation
534 occurred around the injury site where the canals merged at 24 hpa (Fig 2H).

535 These results suggest that blastema is formed around the injury site regardless
536 of the location of amputation.
537 Based on these observations, we hypothesized that blastema is a
538 prerequisite for proper regeneration of the tentacle. To test this possibility, we
539 examined whether blastema formation occurs in the isolated tentacle, which
540 fails to regenerate basal tissue (S1G-S1H Fig). In the isolated tentacle, EdU^+
541 cells were not detected at the injury site at 24 hpa (Fig 2I). These results
542 together suggest that blastema formation is associated solely with the
543 regenerating tentacle.
544
545 **Stem cells compose blastema**
546 What cell types constitute blastema? In hydrozoans, i-cells behave as pluri-
547 /multipotent stem cells that can differentiate into progenitors and differentiated
548 lineages [45]. In order to confirm the cell types that form blastema, we utilized
549 the combination of β-catenin antibody staining and nuclear staining, which can
550 distinguish i-cells, nematocytes, and epithelial cells (Fig 3A). In both *Hydractinia*
551 and *Cladonema*, i-cells were identified by cytoplasmic signals of β-catenin,
552 together with the large nucleus-to-cytoplasm ratio and prominent nucleoli
553 [39,46]. While nematocytes exhibit crescent-shaped nuclei, epithelial cells show
554 a polygonal shape delineated by the membrane-localized β-catenin (Fig 3Aiii).
555 Through the quantification of cell types, we found that around 80% of blastema
556 cells were i-cells, 10% were epithelial cells, and 10% were nematocytes (Fig 3A
557 and 3B), indicating that most cells in blastema are morphologically i-cells.
558 To molecularly characterize these blastema cells, we examined the
559 expression of the stem cell markers, *Nanos1*, *Piwi*, and *Vasa1* by fluorescent *in*
560 *situ* hybridization (FISH). Note that, while *Cladonema* possess two *Nanos*
561 genes, *Nanos1* and *Nanos2, Nanos2*$^+$ cells co-express a nematoblast marker
562 *Mcol1*, suggesting that *Nanos2* is a nematoblast marker rather than a stem cell
563 marker in *Cladonema* medusa (S3E and S3F Fig), similar to *Hydractinia* [47]. In
564 the intact tentacle, *Nanos1*$^+$, *Piwi*$^+$ or *Vasa1*$^+$ cells, are primarily distributed in
565 the bulb and branching site (Figs 3Ci and S3A-S3D, S4Ai, S4Bi) [38,39]. By
566 contrast, at 24 hpa *Nanos1*$^+$ cells accumulated around the injury site where
567 blastema formed (Fig 3Cii), and *Piwi*$^+$ and *Vasa1*$^+$ cells were also localized in
568 the blastema region (S4Aii and S4Bii Fig). While *Nanos1*$^+$ cells accumulated to
569 the new branching bud after 48 hpa (Fig 3Ciii, white arrow) [38,39], *Nanos1*
570 expression was no longer detected at the regenerating tip and was restricted to

571 the middle and basal side of the tentacle (Fig 3Ciii). We further quantified the
572 distribution of *Nanos1*$^{+}$ cells and found a gradual transition of their distribution
573 from the distal to the basal side of the regenerating tentacle (Fig 3D). These
574 results are consistent with the distribution pattern of proliferative cells (Figs 2A-
575 2C and S2A-S2B), further supporting the idea that proliferative cells in blastema
576 exhibit characteristics of stem cells.
577
578 **Most blastema cells are not derived from resident stem cells localized at**
579 **the bulb**
580 Previous reports on cnidarian regeneration have suggested that undifferentiated
581 blastema cells are supplied by the migration of resident stem/progenitor cells in
582 response to injury [20,21,27]. To test whether resident stem cells, or originally-
583 localized i-cells, in the bulb migrate to the injury site to form blastema, we
584 performed EdU-chase experiments during *Cladonema* tentacle regeneration.
585 We leveraged the fact that short-time incubation of EdU labels proliferating i-
586 cells in the intact tentacle, and, after incubating, amputated and visualized the
587 regenerating tentacle at different time points (S5A Fig). Until 24 hpa, most EdU^{+}
588 cells remained localized to the bulb while a small number of EdU^{+} cells were
589 distributed near blastema (S5Ai-vi and S5B Fig). Following 48 h and 72 h
590 chasing, EdU^{+} cells continued to localize at the basal side, including the bulb,
591 rather than in the regenerating tip, although the population of EdU^{+} cells
592 propagated in the distal direction, likely through cell proliferation and migration
593 (S5Avii and S5Aviii Fig). Considering the minimal contribution of EdU^{+} i-cells to
594 blastema, these observations suggest that resident stem cells localized at the
595 bulb may not be sufficient to form blastema.
596 We further conducted an alternative tracing experiment that specifically
597 labels cells in the bulb region by DiI microinjection followed by amputation and
598 cell tracking, which allows monitoring the labeled cells *in vivo* during tentacle
599 regeneration (S6 Fig). To confirm the cell-type of DiI^{+} cells in the bulb, we first
600 combined EdU staining or β-catenin antibody staining with DiI injection (S6A-
601 S6C Fig) to show that more than 75% of EdU^{+} cells or i-cells (β-catenin
602 cytoplasm signal) were DiI^{+} in the bulb (S6A-S6C Fig), indicating that the
603 majority of resident i-cells are labeled by DiI injection. After a 24 h chase, DiI^{+}
604 cells were still localized near the bulb, not merged with EdU^{+} cells in blastema
605 (S6D and S6Ei-ii Fig). In contrast, when DiI was injected into the central area
606 near the amputation site, DiI^{+} cells overlapped with EdU^{+} cells, participating in

607 blastema formation (S6D and S6Eiii-iv Fig). These results, taken together with
608 the EdU chase results, suggest that resident stem cells do not migrate to the
609 blastema region.
610 The above experiments support the presence of two populations of
611 proliferative cells during regeneration: one population are the “resident
612 homeostatic stem cells (RHSCs),” composed of i-cells localized at the bulb, and
613 the other are “repair-specific proliferative cells (RSPCs)” that appear as
614 blastema upon amputation. In order to test this hypothesis, we performed
615 chasing experiments by labeling the two proliferative cell populations with
616 distinct nucleoside analogs, EdU and BrdU (Fig 4A). This approach has been
617 utilized in different animal systems as a way to track proliferative cell
618 populations and their lineages [48–50]. We labeled RHSCs in the bulb by EdU
619 before amputation and RSPCs in the blastema by BrdU at 24 hpa (Fig 4A). At
620 the time of blastema formation at 24 hpa, EdU^+ RHSCs were still localized to
621 the bulb, while $BrdU^+$ RSPCs accumulated at the blastema (Fig 4Bi).
622 Importantly, only 13.6% of $BrdU^+$ RSPCs were EdU^+ in blastema, supporting the
623 notion that the migration of RHSCs may not be sufficient to form blastema (Fig
624 4Bi, 4Cii, and 4D). Indeed, following 24-48 h, $BrdU^+$ RSPCs were distributed on
625 the distal side of the regenerating tentacle, EdU^+ RHSCs remained localized on
626 the basal side, although their distribution expanded slightly (Fig 4Bii and 4Biii).
627 Consistent with these observations, when DiI was injected to the center area
628 near the injury site, these DiI^+ cells initially contributed to RSPCs and were
629 gradually distributed to distal side in the regenerating tentacle (Figs 4Bii, 4Biii
630 and S6H-S6I). These results suggest that RSPCs at the blastema participate in
631 the formation of the new structure while RHSCs expand locally, supporting the
632 existence of two distinct proliferative cell populations during tentacle
633 regeneration (Fig 4G).
634 To determine the characteristics of these distinct proliferative cell
635 populations, we examined their respective proliferative capacities. For this
636 purpose, we quantified the increase in cell numbers of the two populations
637 during tentacle regeneration. At 24 hpa, RHSCs increased approximately two-
638 fold, but no dramatical increase was observed in the following 48 h (Fig 4E; 0
639 hpa: n=206±66.6, 24 hpa: n=441.3±100.6, 48 hpa: n=493.3±123.2, 72 hpa:
640 n=593.7±250.3). Notably, the number of these RHSCs also increased during 24
641 h without amputation (S5C and S5D Fig), suggesting that the increase of
642 RHSCs is not an injury-specific response. In contrast, the number of RSPCs in

643 the blastema tripled at 48 h, which led to an approximate 4-fold increase at 72
644 hpa (Fig 4F; 24 hpa: n=275.1±64.2, 48 hpa: n=929.3±151.9, 72 hpa:
645 n=1125±225.1). These results indicate a pronounced difference in proliferative
646 activity between the two populations, further implicating their distinct responses
647 to injury.
648 If RSPCs do not derive from RHSCs in the bulb, blastema should form
649 when such stem cells are removed. To test this possibility, we examined
650 blastema formation after RHSCs are eliminated by X-ray irradiation. We first
651 determined a condition that would eliminate resident stem cells after exposure
652 to different doses of X-ray irradiation (30, 50, 75 Gy) by monitoring expression
653 of the stem cell marker *Nanos1*. FISH staining of *Nanos1* showed that *Nanos1*$^+$
654 cells decreased in an X-ray dose dependent manor, and most *Nanos1*$^+$ cells
655 were removed at 75 Gy at 3 days post-irradiation (dpi) (S7A-S7C Fig). qPCR
656 analysis further confirmed a significant reduction of *Nanos1* mRNA levels at 3
657 dpi (S7G Fig). We thus amputated the tentacle at 3 dpi and investigated
658 blastema formation by EdU pulse labeling (Fig 4H). At 24 hpa, blastema formed
659 successfully regardless of X-ray irradiation, although the rate of EdU$^+$ cells in
660 the blastema decreased slightly (Fig 4I and 4J). In order to support the
661 conclusion derived from X-ray irradiation, we also performed pharmacological
662 treatments using hydroxyurea (HU) or Mitomycin C, both of which are used to
663 eliminate i-cells in other hydrozoan species [20,51,52]. The results of FISH and
664 qPCR confirmed that most *Nanos1*$^+$ cells are removed by HU or Mitomycin C
665 treatment for 3 days (Fig S7D-S7G). We then examined blastema formation
666 after HU or Mitomycin C treatment and found that blastema formed at 24 hpa,
667 consistent with the results of X-ray irradiation (Fig 4I and 4J). Combined, these
668 results demonstrate that distinct proliferative cell populations appear during
669 tentacle regeneration and that most blastema cells are not derived from
670 RHSCs.
671
672 **RHSCs contribute to nematogenesis and tentacle elongation**
673 In the tentacles of hydrozoan medusae such as *Clytia* and *Cladonema*,
674 proliferative i-cells in the bulb are proposed to migrate from the basal to the
675 distal side while differentiating into nematocytes, which is known as the belt
676 conveyor model [24,37,53]. Based on this proposed model, we hypothesized
677 that RHSCs in the bulb contribute to nematogenesis during both homeostasis
678 and regeneration. In order to test this hypothesis, we performed EdU and BrdU

679 double chase experiments with some modifications (Fig 5A). We found that
680 long-incubation with EdU for 24 h allows for the labeling of RHSCs in the bulb
681 as well as nematocyte progenitors labeled by *Mcol1* (Figs 5Bi and S8). After
682 EdU labeling for 24 h, followed by amputation, most EdU^+ cells remained in the
683 bulb, and 26.9% of the $BrdU^+$ RSPCs were EdU^+ in the blastema, indicating that
684 the majority of RSPCs are of different lineage than RHSCs (Fig 5Bii, 5Biv, and
685 5C). This result is consistent with the results of the chasing experiment using
686 short duration EdU labeling (Fig 4A-4D), further supporting the conclusion that
687 the migration of RHSCs in the bulb is not sufficient to form blastema. At 72 hpa,
688 while EdU^+ cells were still distributed in the basal region, including the bulb,
689 some EdU^+ cells were located in the distal nematocyte clusters (Fig 5Bv: yellow
690 arrow), suggesting that one of the lineages of RHSCs are nematocytes during
691 regeneration. We also performed DiI labeling of the bulb to show that these DiI^+
692 cells were distributed in nematocyte clusters in the regenerated tentacle (S6F
693 and S6G Fig: white arrow).
694 To further confirm the above observations, we identified cell types
695 located in the distal side of the tentacle. We found that atypical protein kinase C
696 (aPKC) antibody can be utilized to detect cell types with nuclear staining, which
697 is a method similar to using β-catenin antibody (Figs 3A, 5D and S9) [39,46].
698 The combination of EdU chasing and cell type identification revealed that nearly
699 half of the EdU^+ cells are nematocytes in the distal side of the tentacle
700 (nematocytes: 45.7%, epithelial cells: 24.2%, i-cells: 30.1%; Fig 5E-5G). These
701 results together indicate that RHSCs in the bulb differentiate into nematocytes
702 during regeneration. Intriguingly, we also noticed that EdU-labeled RHSCs
703 merged with $FMRFamide^+$ neurons (S10A and S10B Fig), suggesting that
704 RHSCs can differentiate into neurons during tentacle regeneration.
705 Given that the RHSCs mainly differentiate into both nematocytes and
706 epithelial cells during regeneration (Fig 5F and 5G), it is expected that these
707 cells play a role in supplying new nematocytes as well as in tentacle elongation.
708 We first examined the timing of nematocyte cluster formation as a readout of
709 nematogenesis when RHSCs were eliminated by X-ray or drug treatments
710 using HU or Mitomycin C (Fig 5H-5J) and found that it was delayed, particularly
711 at the early stage of regeneration after elimination of RHSCs (Fig 5I and 5J),
712 indicating that RHSCs migrate from the basal to the distal side while
713 differentiating into nematocytes during regeneration.

714 Next, we measured tentacle length during regeneration with RHSCs
715 cells removed by X-ray irradiation or drug treatments (Fig 5H and 5K). When
716 tentacles were amputated at 3 dpi by which time RHSCs had been eliminated
717 by X-ray, tentacle elongation was severely inhibited compared to the non-
718 irradiated controls (Fig 5K, regenerated tentacle length at 4 dpa, Control: 1.66
719 mm, X-ray: 0.540 mm). It is possible that X-ray irradiation affects the source of
720 RSPCs to some extent, and indeed when RHSCs were removed with HU or
721 Mitomycin C treatment, tentacle elongation was mildly but still significantly
722 inhibited (Fig 5K, regenerated tentacle length at 4 dpa, HU: 1.14 mm, Mitomycin
723 C: 1.19 mm). Given that EdU^+ blastema cells appear after X-ray irradiation as
724 well as drug treatments (Fig 4I and 4J), RHSCs contribute to tentacle elongation
725 independently of blastema cells. We speculate that RHSCs, and particularly
726 their decedents, participate in tissue elongation likely through pushing out from
727 the basal side as progenitors and differentiating into epithelial cells.
728
729 **RSPCs contribute to reconstruction of the new tentacle**
730 In order to investigate the role of RSPCs during regeneration, we performed
731 EdU chase labeling of the blastema with cell type identification by aPKC
732 antibody staining (Fig 6A-6C). While 94.4% of the RSPCs exhibited i-cell
733 morphology at 24 hpa (Fig 6Bi, 6Biii and 6C, consistent with the results of β-
734 catenin antibody staining in Fig 3A and 3B), 59.2% of EdU^+ cells were epithelial
735 cells in the distal portion of the regenerating tentacle at 72 hpa, (Fig 6Bii, 6Biv
736 and 6C). Strikingly, in contrast to RHSCs, EdU^+ cells derived from the blastema
737 did not become nematocytes (Fig 5E-5G and 6A-6C). These results suggest
738 that RSPCs preferentially differentiate into epithelial cells in the regenerating
739 tentacle. Of note, we found that a small portion of EdU-labeled RSPCs merged
740 with $FMRFamide^+$ neurons, although these populations are significantly smaller
741 than the RHSCs (S10C-S10E Fig). Combined, these findings indicate that
742 RSPCs are multipotent, or at least bipotent, stem cells that preferentially
743 generate epithelial cells during regeneration.
744 To identify the role of RSPCs, we examined the impact of locally
745 inhibiting cell proliferation on tentacle regeneration (Figs 6D-6I and S11). UVA
746 radiation (320 to 400 nm) induces various forms of cellular damage via the
747 production of reactive oxygen species or the impairment of proteasomal
748 function, which blocks cell cycle progression at the G_2/M phase in both
749 mammalian cultured cells and fly epidermal progenitors [54–57]. In addition,

750 Hoechst and BrdU are known photosensitizers [58,59], which can facilitate the
751 process of damage induction. To verify the effects of UVA on RSPCs, we
752 performed UV laser illumination around the blastema region at 25 hpa and
753 counted the number of EdU labeled cells (Fig 6D-6F). Following around 24-48
754 h, the number of EdU^+ cells decreased significantly in the UV exposed tentacle
755 compared to the control, indicating that UV laser exposure inhibits cell
756 proliferation of RSPCs (Fig 6F). In contrast, we confirmed that cell proliferation
757 and the timing of nematocyte cluster formation by RHSCs were similar to the
758 non-UV exposure controls, suggesting a minimal impact of UV laser exposure
759 on RHSCs (S11 Fig). In order to examine the contribution of the proliferation of
760 RSPCs toward tentacle regeneration, we monitored the length of regenerating
761 tentacles after UV laser exposure (Fig 6G). Upon UV laser illumination, tentacle
762 elongation during regeneration was significantly inhibited (Fig 6H and 6I). These
763 results, together with the distribution of their descendants on the distal side of
764 the regenerating tentacle (Fig 4Biii and 5Biii), indicate that proliferation of
765 RSPCs contribute to the reconstruction of new tentacles after amputation.
766
767
768 ## Discussion
769 In this study, we uncovered the cellular mechanism underlying blastema
770 formation during *Cladonema* tentacle regeneration. We found that, upon
771 amputation of the tentacle, RSPCs accumulate as blastema, most of which is
772 not derived from RHSCs. While RHSCs contribute to nematogenesis and tissue
773 elongation during both homeostasis and regeneration, RSPCs differentiate into
774 the epithelial cells of the newly formed tentacle. Based on these results, we
775 propose that distinct proliferative cell populations facilitate rapid functional
776 regeneration of the tentacle, which enables critical behaviors of jellyfish
777 organismal physiology such as feeding and swimming (Fig 7A).
778
779
780 **Heterogeneity of stem-like cells**
781 In hydrozoans, i-cells behave as pluripotent or multipotent stem cells that can
782 differentiate into several progenitors and differentiated lineages such as
783 nematocytes, neurons, gland cells, and gametes. Although i-cells exhibit
784 common features such as their interstitial localization, cellular morphology, and
785 expression of the conserved stem cell markers (*Nanos, Piwi, Vasa, PL10*); their

786 potency and heterogeneity likely differ across species [45]. Indeed, *Hydra* i-cells
787 differentiate into most cell types except epithelial cells, while *Hydractinia* i-cells
788 behave as pluripotent cells that can differentiate into all cell types including
789 somatic and germline cells [16,60,61].
790 In the intact *Cladonema* jellyfish, *Nanos1*$^+$, *Piwi*$^+$, and *Vasa1*$^+$ cells are
791 primarily distributed at the bulb (Figs 3C and S4A, S4B), and about 70% of
792 RHSCs in the bulb are *Nanos1*$^+$ cells (Fig 3E and 3F). From lineage-tracing
793 experiments, these RHSCs differentiate into epithelia as well as nematocytes
794 (Fig 5F and 5G), suggesting their role as multipotent stem cells. These
795 observations are consistent with the jellyfish *Clytia*, in which i-cells in the bulb
796 proliferate and differentiate into nematocytes [37,53], indicating that i-cells in the
797 tentacle bulb are commonly involved in organ homeostasis including
798 nematogenesis in hydrozoan jellyfish.
799 In contrast to RHSCs in the bulb, only 17-36% of RSPCs at blastema
800 express *Nanos1*$^+$, *Piwi*$^+$, and *Vasa1*$^+$ (Figs 3E-3F and S4C-S4E), although more
801 than 80% of blastema cells show i-cell morphology (Fig 3A-3B and 6B-6C).
802 These results imply that the stem-like population of the blastema is likely
803 heterogenous, and differs from that of resident i-cells in the bulb. Indeed,
804 RSPCs predominantly differentiate into epithelial cells rather than nematocytes
805 (Fig 6A-6C), suggesting their role as lineage-restricted stem/progenitor cells
806 while maintaining the potential to become neurons in the regenerating tentacle
807 (S10 Fig). Such stem-like cells also accumulate at the newly-formed branch
808 starting at 48-72 hpa (Fig 4Bii-iii), consistent with the prediction by the previous
809 report proposing that i-cell population in the branching bud differs from RHSCs
810 in the bulb [39]. While previous studies using other cnidarians have described
811 active cell proliferation upon injuries, these proliferating cells are
812 pluri/multipotent stem cells migrating to the injury site [20,21,27,62], not lineage-
813 restricted stem/progenitor cells like RSPCs. Altogether, our findings support the
814 heterogeneity of stem-like cells in *Cladonema* jellyfish (Fig 7A), which is similar
815 to the subpopulations of *Hydra* i-cells [52,63].
816
817
818 **How are RSPCs supplied in the blastema?**
819 Our work is the first to demonstrate that RSPCs, which exhibit preferential
820 differentiation into epithelial cells, appear upon injury in cnidarians, but how this
821 cell population is supplied remains unknown. Lineage-tracing experiments,

822 together with the elimination of RHSCs show that blastema formation is mostly
823 independent of RHSCs in the bulb (Figs 4 and S6). When the distal side of the
824 tentacle, where few proliferating cells exist, is amputated, local cell proliferation
825 is still observed around the injury site (Fig 2G). These observations raise two
826 possibilities: mitotic re-entry of quiescent/slow-cycling stem cells or
827 dedifferentiation from differentiated cells into stem-like cells.
828 Previous reports have showed that some cnidarian species possess
829 quiescent or slow-cycling stem cells. For instance, while *Hydra* has three types
830 of adult stem cells—i-cells, epidermal stem cells, and gastrodermis epithelial
831 stem cells—the subpopulation of each stem cell is slow-cycling [52]. These
832 slow-cycling cells are resistant to hydroxyurea treatment due to G2 phase
833 arrest, and re-enter the cell cycle during head regeneration. *Nematostella* also
834 has slow-cycling/quiescent cells that are predominantly present in the
835 mesenteries and are resistant to X-ray irradiation, and these cells' cell cycle is
836 activated upon injury, when they migrate toward the wound site [21]. Given that
837 a small number of i-cells exist in the *Cladonema* intact tentacle, outside the
838 bulb, and branching bud (Figs 3C and S3A, S3C, S3D, S4A, S4B)[39]; such a
839 minor population of i-cells may behave as slow-cycling/quiescent cells and re-
840 enter the cell cycle in response to injury.
841 By contrast, although cnidarian dedifferentiation potential is still debated,
842 some species appear to exhibit context-dependent cellular plasticity [64]. For
843 instance, classical experiments using the hydrozoan jellyfish *Podocoryna*
844 *carnea* have indicated their dedifferentiation potential *in vitro*: when isolated
845 striated muscles are cultured after collagenase treatment, the muscle cells
846 dedifferentiate into stem-like cells and re-differentiate into multiple cell types
847 [65]. Additionally, in green *Hydra*, the isolated gastrodermis, which is i-cell free,
848 can reconstitute a complete polyp including the epidermis [66]. In this case,
849 gastrodermal gland cells appear to dedifferentiate into i-cells [67], while
850 gastrodermal digestive cells transdifferentiate into epidermal epitheliomuscular
851 cells [68]. Moreover, a recent report using *Hydractinia* has shown that, when the
852 hypostome is isolated from the body, cellular reprogramming triggered by cell
853 senescence occurs in somatic cells, which convert into pluripotent *Piwi1*$^{+}$ i-cells
854 [69]. Although these reports support the possibility that dedifferentiation
855 produces pluri/multipotent stem cells after isolation from the body, it is also
856 possible that RSPCs are derived from their descendant cell types. During newt
857 limb regeneration, cellular lineage is restricted such that muscle progenitors

858 dedifferentiated from resident muscle fibers produce only muscles [7,70]. Given
859 that repair-specific proliferative cells in the *Cladonema* tentacle mainly
860 differentiate into epithelial cells (Fig 6A-6C), epithelial cells may dedifferentiate
861 into progenitors that give rise to epithelial cells in the newly formed tentacle.
862
863 **Evolutionary conservation and diversification of blastema formation**
864 Although the molecular and cellular mechanisms of animal regeneration have
865 been addressed in detail using representative species such as planaria and
866 salamanders, questions such as the evolutionary history of regeneration and
867 the homology of regeneration mechanisms across species remain largely
868 unknown. Repair-specific stem cells provided by quiescent stem cells and/or
869 dedifferentiation are common blastema components in bilaterian appendage
870 regeneration. As in vertebrates where lineage-restricted repair-specific
871 stem/progenitor cells participate in appendage regeneration [7,9,11], the
872 protostome ecdysozoa *Parhyale hawaiensis* utilize re-activation of muscle
873 satellite cells during thoracic leg regeneration [71]. By contrast, during
874 echinoderm starfish arm regeneration, dedifferentiated dermal cells form
875 blastema-like structures [72]. Similarly, during insect cricket leg regeneration,
876 the source of blastemal cells is derived from injury-induced dedifferentiation
877 [73,74]. These reports suggest that repair-specific production of blastema cells
878 is relatively conserved throughout bilaterians (Fig 7B).
879 In non-bilaterian metazoans, resident pluripotent stem cells are thought
880 to contribute to both homeostasis and whole-body regeneration. During the
881 regeneration of the demosponge in Porifera, one of the most primitive animals,
882 archeocytes known as homeostatic stem cells contribute to an undifferentiated
883 cell mass beneath the wound as a blastema-like structure [75]. While the
884 regenerating ctenophore cydippids do not apparently form blastema-like
885 structure, slow-cycling stem-like cells are recruited to the injury site [76]. In
886 cnidarians, resident stem cells, which are involved in homeostasis, are recruited
887 to the injury site after amputation of the body and removal of the organs [19–
888 21,27]. By contrast, as shown in this study, the main cellular source of
889 blastemal cells is not RHSCs but rather RSPCs during *Cladonema* tentacle
890 regeneration (Fig 4). Our findings suggest that, in terms of the regeneration
891 processes and blastemal cellular source, the regeneration mechanism of the
892 *Cladonema* tentacle is more similar to that of bilaterian species (Fig 7B).

One important remaining question is whether bilaterians' and cnidarians' most recent common ancestor possessed a system to supply blastema through repair-specific stem/proliferative cells. Although sponges and ctenophores have been proposed to possess dedifferentiation or transdifferentiation potentials that can provide a cellular source of regenerated bodies [64], it is currently unknown whether they are repair-specific cell populations or not. In this study, we demonstrate that RSPCs contribute to the newly generated epithelium during *Cladonema* tentacle regeneration. Intriguingly, recent genomic studies have revealed that jellyfish-specific genes are not conserved among bilaterians or even other cnidarians including corals and sea anemones, and the anthozoan *Nematostella* is the most 'bilaterian-like' cnidarian sequenced [77–79]. These findings raise the possibility that medusozoans had evolved the medusa stage after branching from their common ancestor and that bilaterians and cnidarian jellyfish likely independently acquired a similar mechanism of blastema formation upon amputation of appendages. It is thus tempting to speculate that blastema formation by RSPCs is a common feature acquired for complex organ and appendage regeneration during animal evolution.

References

1. McCusker C, Bryant SV, Gardiner DM. The axolotl limb blastema: cellular and molecular mechanisms driving blastema formation and limb regeneration in tetrapods: The Axolotl Limb Blastema. Regeneration. 2015;2: 54–71. doi:10.1002/reg2.32
2. Seifert AW, Muneoka K. The blastema and epimorphic regeneration in mammals. Developmental Biology. 2018;433: 190–199. doi:10.1016/j.ydbio.2017.08.007
3. Aztekin C. Appendage regeneration is context dependent at the cellular level. Open Biol. 2021;11: 210126. doi:10.1098/rsob.210126
4. Bely AE, Nyberg KG. Evolution of animal regeneration: re-emergence of a field. Trends in Ecology & Evolution. 2010;25: 161–170. doi:10.1016/j.tree.2009.08.005
5. Tanaka EM, Reddien PW. The Cellular Basis for Animal Regeneration. Developmental Cell. 2011;21: 172–185. doi:10.1016/j.devcel.2011.06.016

927 6. Reddien PW, Alvarado AS. FUNDAMENTALS OF PLANARIAN
928 REGENERATION. Annu Rev Cell Dev Biol. 2004;20: 725–757.
929 doi:10.1146/annurev.cellbio.20.010403.095114
930 7. Sandoval-Guzmán T, Wang H, Khattak S, Schuez M, Roensch K, Nacu E, et
931 al. Fundamental Differences in Dedifferentiation and Stem Cell Recruitment during
932 Skeletal Muscle Regeneration in Two Salamander Species. Cell Stem Cell. 2014;14:
933 174–187. doi:10.1016/j.stem.2013.11.007
934 8. Ando K, Shibata E, Hans S, Brand M, Kawakami A. Osteoblast Production by
935 Reserved Progenitor Cells in Zebrafish Bone Regeneration and Maintenance.
936 Developmental Cell. 2017;43: 643-650.e3. doi:10.1016/j.devcel.2017.10.015
937 9. Knopf F, Hammond C, Chekuru A, Kurth T, Hans S, Weber CW, et al. Bone
938 Regenerates via Dedifferentiation of Osteoblasts in the Zebrafish Fin. Developmental
939 Cell. 2011;20: 713–724. doi:10.1016/j.devcel.2011.04.014
940 10. Daponte V, Tylzanowski P, Forlino A. Appendage Regeneration in
941 Vertebrates: What Makes This Possible? Cells. 2021;10: 242.
942 doi:10.3390/cells10020242
943 11. Lehoczky JA, Robert B, Tabin CJ. Mouse digit tip regeneration is mediated by
944 fate-restricted progenitor cells. Proc Natl Acad Sci USA. 2011;108: 20609–20614.
945 doi:10.1073/pnas.1118017108
946 12. Fritz AE, Ikmi A, Seidel C, Paulson A, Gibson MC. Mechanisms of tentacle
947 morphogenesis in the sea anemone *Nematostella vectensis*. Development. 2013;140:
948 2212–2223. doi:10.1242/dev.088260
949 13. Technau U, Steele RE. Evolutionary crossroads in developmental biology:
950 Cnidaria. Development. 2011;138: 1447–1458. doi:10.1242/dev.048959
951 14. Fujita S, Kuranaga E, Nakajima Y. Regeneration Potential of Jellyfish: Cellular
952 Mechanisms and Molecular Insights. Genes. 2021;12: 758. doi:10.3390/genes12050758
953 15. Holstein TW, Hobmayer E, Technau U. Cnidarians: An evolutionarily
954 conserved model system for regeneration? Dev Dyn. 2003;226: 257–267.
955 doi:10.1002/dvdy.10227
956 16. Gahan JM, Bradshaw B, Flici H, Frank U. The interstitial stem cells in
957 Hydractinia and their role in regeneration. Current Opinion in Genetics & Development.
958 2016;40: 65–73. doi:10.1016/j.gde.2016.06.006
959 17. Röttinger E. Nematostella vectensis, an Emerging Model for Deciphering the
960 Molecular and Cellular Mechanisms Underlying Whole-Body Regeneration. Cells.
961 2021;10: 2692. doi:10.3390/cells10102692

962 18. Vogg MC, Galliot B, Tsiairis CD. Model systems for regeneration: Hydra.
963 Development. 2019;146. doi:10.1242/dev.177212
964 19. Chera S, Ghila L, Dobretz K, Wenger Y, Bauer C, Buzgariu W, et al.
965 Apoptotic Cells Provide an Unexpected Source of Wnt3 Signaling to Drive Hydra Head
966 Regeneration. Developmental Cell. 2009;17: 279–289.
967 doi:10.1016/j.devcel.2009.07.014
968 20. Bradshaw B, Thompson K, Frank U. Distinct mechanisms underlie oral vs
969 aboral regeneration in the cnidarian Hydractinia echinata. eLife. 2015;4: e05506.
970 doi:10.7554/eLife.05506
971 21. Amiel AR, Foucher K, Ferreira S, Röttinger E. Synergic coordination of stem
972 cells is required to induce a regenerative response in anthozoan cnidarians. bioRxiv;
973 2019. p. 2019.12.31.891804. doi:10.1101/2019.12.31.891804
974 22. Katsuki T, Greenspan RJ. Jellyfish nervous systems. Current Biology. 2013;23:
975 R592–R594. doi:10.1016/j.cub.2013.03.057
976 23. Leclère L, Röttinger E. Diversity of Cnidarian Muscles: Function, Anatomy,
977 Development and Regeneration. Front Cell Dev Biol. 2017;4.
978 doi:10.3389/fcell.2016.00157
979 24. Fujita S, Kuranaga E, Nakajima Y. Cell proliferation controls body size
980 growth, tentacle morphogenesis, and regeneration in hydrozoan jellyfish *Cladonema*
981 *pacificum*. PeerJ. 2019;7: e7579. doi:10.7717/peerj.7579
982 25. Gamero-Mora E, Halbauer R, Bartsch V, Stampar SN, Morandini AC.
983 Regenerative Capacity of the Upside-down Jellyfish Cassiopea xamachana. Zool Stud.
984 2019;58. doi:10.6620/ZS.2019.58-37
985 26. Ostendarp M, Plewka J, Flathmann J, Tilstra A, El-Khaled YC, Wild C.
986 Complete and rapid regeneration of fragments from the upside-down jellyfish
987 Cassiopea. Front Mar Sci. 2022;9: 949233. doi:10.3389/fmars.2022.949233
988 27. Sinigaglia C, Peron S, Eichelbrenner J, Chevalier S, Steger J, Barreau C, et al.
989 Pattern regulation in a regenerating jellyfish. eLife. 2020;9: e54868.
990 doi:10.7554/eLife.54868
991 28. Stamatis S-A, Worsaae K, Garm A. Regeneration of the Rhopalium and the
992 Rhopalial Nervous System in the Box Jellyfish *Tripedalia cystophora*. The Biological
993 Bulletin. 2018;234: 22–36. doi:10.1086/697071
994 29. Stierwald M, Yanze N, Bamert RP, Kammermeier L, Schmid V. The Sine
995 oculis/Six class family of homeobox genes in jellyfish with and without eyes:
996 development and eye regeneration. Developmental Biology. 2004;274: 70–81.
997 doi:10.1016/j.ydbio.2004.06.018

30. Weber C. Structure, histochemistry, ontogenetic development, and regeneration of the ocellus ofCladonema radiatum dujardin (cnidaria, hydrozoa, anthomedusae). J Morphol. 1981;167: 313–331. doi:10.1002/jmor.1051670306

31. Fujiki A, Hou S, Nakamoto A, Kumano G. Branching pattern and morphogenesis of medusa tentacles in the jellyfish Cladonema pacificum (Hydrozoa, Cnidaria). Zoological Lett. 2019;5: 12. doi:10.1186/s40851-019-0124-4

32. Masuda-Ozawa T, Fujita S, Nakamura R, Watanabe H, Kuranaga E, Nakajima Y. siRNA-mediated gene knockdown via electroporation in hydrozoan jellyfish embryos. Sci Rep. 2022;12: 16049. doi:10.1038/s41598-022-20476-1

33. Takeda N, Kon Y, Artigas GQ, Lapébie P, Barreau C, Koizumi O, et al. Identification of jellyfish neuropeptides that act directly as oocyte maturation-inducing hormones. Development. 2018;145. doi:10.1242/dev.156786

34. Rees JT. The polyp and immature medusa stages of *Cladonema californicum* , Hyman, 1947 (Anthomedusae: Cladonemidae) with biological notes and a discussion of the taxonomy of the genus *Cladonema*. Journal of Natural History. 1979;13: 295–302. doi:10.1080/00222937900770231

35. Suga H, Schmid V, Gehring WJ. Evolution and Functional Diversity of Jellyfish Opsins. Current Biology. 2008;18: 51–55. doi:10.1016/j.cub.2007.11.059

36. Zhou K, Gu Y, Wang L, Chen J. Discovery of Cladonema multiramosum sp. nov. (Cnidaria: Hydrozoa: Cladonematidae) using DNA barcoding and life cycle analyses. Acta Oceanol Sin. 2022;41: 44–52. doi:10.1007/s13131-021-1900-5

37. Denker E, Manuel M, Leclère L, Le Guyader H, Rabet N. Ordered progression of nematogenesis from stem cells through differentiation stages in the tentacle bulb of Clytia hemisphaerica (Hydrozoa, Cnidaria). Developmental Biology. 2008;315: 99–113. doi:10.1016/j.ydbio.2007.12.023

38. Fujita S, Kuranaga E, Miura M, Nakajima Y-I. Fluorescent In Situ Hybridization and 5-Ethynyl-2'-Deoxyuridine Labeling for Stem-like Cells in the Hydrozoan Jellyfish Cladonema pacificum. J Vis Exp. 2022. doi:10.3791/64285

39. Hou S, Zhu J, Shibata S, Nakamoto A, Kumano G. Repetitive accumulation of interstitial cells generates the branched structure of *Cladonema* medusa tentacles. Development. 2021;148: dev199544. doi:10.1242/dev.199544

40. Passamaneck YJ, Martindale MQ. Cell proliferation is necessary for the regeneration of oral structures in the anthozoan cnidarian Nematostella vectensis. BMC Dev Biol. 2012;12: 34. doi:10.1186/1471-213X-12-34

1032 41. Galliot B, Buzgariu W, Schenkelaars Q, Wenger Y. Non-developmental
1033 dimensions of adult regeneration in Hydra. Int J Dev Biol. 2018;62: 373–381.
1034 doi:10.1387/ijdb.180111bg
1035 42. Lesh-Laurie GE, Hujer A, Suchy P. Polyp regeneration from isolated tentacles
1036 of Aurelia scyphistomae: a role for gating mechanisms and cell division. Hydrobiologia.
1037 1991;216: 91–97. doi:10.1007/BF00026448
1038 43. Salic A, Mitchison TJ. A chemical method for fast and sensitive detection of
1039 DNA synthesis *in vivo*. Proc Natl Acad Sci USA. 2008;105: 2415–2420.
1040 doi:10.1073/pnas.0712168105
1041 44. Tasaki J, Shibata N, Sakurai T, Agata K, Umesono Y. Role of c-Jun N-terminal
1042 kinase activation in blastema formation during planarian regeneration: JNK activation in
1043 planarian regeneration. Development, Growth & Differentiation. 2011;53: 389–400.
1044 doi:10.1111/j.1440-169X.2011.01254.x
1045 45. Gold DA, Jacobs DK. Stem cell dynamics in Cnidaria: are there unifying
1046 principles? Dev Genes Evol. 2013;223: 53–66. doi:10.1007/s00427-012-0429-1
1047 46. Plickert G, Frank U, Müller WA. Hydractinia, a pioneering model for stem cell
1048 biology and reprogramming somatic cells to pluripotency. Int J Dev Biol. 2012;56:
1049 519–534. doi:10.1387/ijdb.123502gp
1050 47. Kanska J, Frank U. New roles for Nanos in neural cell fate determination
1051 revealed by studies in a cnidarian. Development. 2013;140: e1608–e1608.
1052 doi:10.1242/dev.101246
1053 48. Harris L, Zalucki O, Piper M. BrdU/EdU dual labeling to determine the cell-
1054 cycle dynamics of defined cellular subpopulations. J Mol Hist. 2018;49: 229–234.
1055 doi:10.1007/s10735-018-9761-8
1056 49. Ribeiro RP, Egger B, Ponz-Segrelles G, Aguado MT. Cellular proliferation
1057 dynamics during regeneration in Syllis malaquini (Syllidae, Annelida). Front Zool.
1058 2021;18: 27. doi:10.1186/s12983-021-00396-y
1059 50. Vega CJ, Peterson DA. Stem cell proliferative history in tissue revealed by
1060 temporal halogenated thymidine analog discrimination. Nat Methods. 2005;2: 167–169.
1061 doi:10.1038/nmeth741
1062 51. Bode HR, Scott Smith G. Regulation of interstitial cell differentiation inHydra
1063 attenuata: II. Correlation of the axial position of the interstitial cell with nematocyte
1064 differentiation. Wilhelm Roux' Archiv. 1977;181: 203–213. doi:10.1007/BF00848421
1065 52. Govindasamy N, Murthy S, Ghanekar Y. Slow-cycling stem cells in hydra
1066 contribute to head regeneration. Biology Open. 2014;3: 1236–1244.
1067 doi:10.1242/bio.201410512

1068 53. Condamine T, Jager M, Leclère L, Blugeon C, Lemoine S, Copley RR, et al.
1069 Molecular characterisation of a cellular conveyor belt in Clytia medusae.
1070 Developmental Biology. 2019;456: 212–225. doi:10.1016/j.ydbio.2019.09.001
1071 54. Catalgol B, Ziaja I, Breusing N, Jung T, Höhn A, Alpertunga B, et al. The
1072 Proteasome Is an Integral Part of Solar Ultraviolet A Radiation-induced Gene
1073 Expression. Journal of Biological Chemistry. 2009;284: 30076–30086.
1074 doi:10.1074/jbc.M109.044503
1075 55. Girard P-M, Pozzebon M, Delacôte F, Douki T, Smirnova V, Sage E.
1076 Inhibition of S-phase progression triggered by UVA-induced ROS does not require a
1077 functional DNA damage checkpoint response in mammalian cells. DNA Repair.
1078 2008;7: 1500–1516. doi:10.1016/j.dnarep.2008.05.004
1079 56. Latonen L, Laiho M. Cellular UV damage responses—Functions of tumor
1080 suppressor p53. Biochimica et Biophysica Acta (BBA) - Reviews on Cancer.
1081 2005;1755: 71–89. doi:10.1016/j.bbcan.2005.04.003
1082 57. Nakajima Y, Kuranaga E, Sugimura K, Miyawaki A, Miura M.
1083 Nonautonomous Apoptosis Is Triggered by Local Cell Cycle Progression during
1084 Epithelial Replacement in Drosophila. Mol Cell Biol. 2011;31: 2499–2512.
1085 doi:10.1128/MCB.01046-10
1086 58. Herweijer H, And WS, Visser JWM. High-speed photodamage cell selection
1087 using bromodeoxyuridine/Hoechst 33342 photosensitized cell killing. Cytometry.
1088 1988;9: 143–149. doi:10.1002/cyto.990090208
1089 59. Singh S, Dwarakanath B, Mathew T. DNA ligand Hoechst-33342 enhances UV
1090 induced cytotoxicity in human glioma cell lines. Journal of Photochemistry and
1091 Photobiology B: Biology. 2004;77: 45–54. doi:10.1016/S1011-1344(04)00122-8
1092 60. Varley Á, Horkan HR, McMahon ET, Krasovec G, Frank U. Pluripotent, germ
1093 cell competent adult stem cells underlie cnidarian plant-like life history. Developmental
1094 Biology; 2022 Nov. doi:10.1101/2022.11.09.515637
1095 61. Watanabe H, Hoang VT, Mättner R, Holstein TW. Immortality and the base of
1096 multicellular life: Lessons from cnidarian stem cells. Seminars in Cell & Developmental
1097 Biology. 2009;20: 1114–1125. doi:10.1016/j.semcdb.2009.09.008
1098 62. Chera S, Ghila L, Wenger Y, Galliot B. Injury-induced activation of the
1099 MAPK/CREB pathway triggers apoptosis-induced compensatory proliferation in hydra
1100 head regeneration: MAPK-dependent injury-induced apoptosis in Hydra. Development,
1101 Growth & Differentiation. 2011;53: 186–201. doi:10.1111/j.1440-169X.2011.01250.x
1102 63. David CN. Interstitial stem cells in Hydra: multipotency and decision-making.
1103 Int J Dev Biol. 2012;56: 489–497. doi:10.1387/ijdb.113476cd

1104 64. Nakanishi N, Jacobs DK. The Early Evolution of Cellular Reprogramming in
1105 Animals. 1st ed. In: Bishop CD, Hall BK, editors. Deferring Development. 1st ed. CRC
1106 Press; 2019. pp. 67–86. doi:10.1201/9780429445446-4
1107 65. Schmid V, Alder H. Isolated, mononucleated, striated muscle can undergo
1108 pluripotent transdifferentiation and form a complex regenerate. Cell. 1984;38: 801–809.
1109 doi:10.1016/0092-8674(84)90275-7
1110 66. Haynes J, Burnett AL. Dedifferentiation and Redifferentiation of Cells in
1111 Hydra viridis. Science. 1963;142: 1481–1483. doi:10.1126/science.142.3598.1481
1112 67. Burnett AL, Davis LE, Ruffing FE. A histological and ultrastructural study of
1113 germinal differentiation of interstitial cells arising from gland cells inHydra viridis. J
1114 Morphol. 1966;120: 1–8. doi:10.1002/jmor.1051200102
1115 68. Davis LE, Burnett AL, Haynes JF, Mumaw VR. A histological and
1116 ultrastructural study of dedifferentiation and redifferentiation of digestive and gland
1117 cells in Hydra viridis. Developmental Biology. 1966;14: 307–329. doi:10.1016/0012-
1118 1606(66)90018-2
1119 69. Salinas-Saavedra M, Febrimarsa, Krasovec G, Horkan HR, Baxevanis AD,
1120 Frank U. Senescence-induced cellular reprogramming drives cnidarian whole-body
1121 regeneration. Cell Reports. 2023;42: 112687. doi:10.1016/j.celrep.2023.112687
1122 70. Tanaka HV, Ng NCY, Yang Yu Z, Casco-Robles MM, Maruo F, Tsonis PA, et
1123 al. A developmentally regulated switch from stem cells to dedifferentiation for limb
1124 muscle regeneration in newts. Nat Commun. 2016;7: 11069. doi:10.1038/ncomms11069
1125 71. Konstantinides N, Averof M. A Common Cellular Basis for Muscle
1126 Regeneration in Arthropods and Vertebrates. Science. 2014;343: 788–791.
1127 doi:10.1126/science.1243529
1128 72. Fan T, Fan X, Du Y, Sun W, Zhang S, Li J. Patterns and cellular mechanisms
1129 of arm regeneration in adult starfish Asterias rollestoni bell. J Ocean Univ China.
1130 2011;10: 255–262. doi:10.1007/s11802-011-1837-y
1131 73. Bando T, Mito T, Hamada Y, Ishimaru Y, Noji S, Ohuchi H. Molecular
1132 mechanisms of limb regeneration: insights from regenerating legs of the cricket Gryllus
1133 bimaculatus. Int J Dev Biol. 2018;62: 559–569. doi:10.1387/ijdb.180048ho
1134 74. Truby PR. Blastema formation and cell division during cockroach limb
1135 regeneration. Development. 1983;75: 14.
1136 75. Borisenko IE, Adamska M, Tokina DB, Ereskovsky AV. Transdifferentiation
1137 is a driving force of regeneration in *Halisarca dujardini* (Demospongiae, Porifera).
1138 PeerJ. 2015;3: e1211. doi:10.7717/peerj.1211

76. Ramon-Mateu J, Ellison ST, Angelini TE, Martindale MQ. Regeneration in the ctenophore Mnemiopsis leidyi occurs in the absence of a blastema, requires cell division, and is temporally separable from wound healing. BMC Biol. 2019;17: 80. doi:10.1186/s12915-019-0695-8

77. Khalturin K, Shinzato C, Khalturina M, Hamada M, Fujie M, Koyanagi R, et al. Medusozoan genomes inform the evolution of the jellyfish body plan. Nat Ecol Evol. 2019;3: 811–822. doi:10.1038/s41559-019-0853-y

78. Putnam NH, Srivastava M, Hellsten U, Dirks B, Chapman J, Salamov A, et al. Sea Anemone Genome Reveals Ancestral Eumetazoan Gene Repertoire and Genomic Organization. Science. 2007;317: 86–94. doi:10.1126/science.1139158

79. Steele RE, David CN, Technau U. A genomic view of 500 million years of cnidarian evolution. Trends in Genetics. 2011;27: 7–13. doi:10.1016/j.tig.2010.10.002

Acknowledgement

We thank R. Deguchi (Miyagi Univ. Education, Japan) for sharing *Cladonema pacificum*. We thank D. Umetsu, H. Nagai and T. Akiyama for helpful discussion. We thank I. Nagai, A. Sasaki, and H. Nakatani for technical assistance and animal maintenance. We thank Y. Nashimoto for technical support. This work was supported by JSPS/MEXT KAKENHI (grant numbers JP21H05767 to G.K., JP21H05255 to E.K., JP21H04774, JP21K19206 to M.M., and JP17H06332, JP22H02762, JP23H04696 to Y.N.), JST grant (JPMJCR1852 to E.K. and JPMJSP2114 to S.F.), AMED-Aging (JP21gm5010001 to M.M.), and AMED-PRIME (JP22gm6110025 to Y.N.), and NIBB Collaborative Research Program (23NIBB202 to Y.N.).

Author contributions

S.F. conceptualized and designed the project, performed experiments, analyzed data, prepared figures, and wrote the manuscript. M.T. performed experiments, and analyzed data. G.K., E.K., and M.M. supervised the project. Y.N. conceptualized, supervised and designed the project, prepared figures, and wrote the manuscript. All authors approved the final manuscript.

Competing interests

The authors declare no competing interests.

Figure legends

Fig 1. Regeneration processes and potentials of the *Cladonema* medusa tentacle. (A) The phylogenetic tree of Bilateria and Cnidaria, composed of Anthozoa and Medusozoa. (B) Medusa of *Cladonema pacificum*. U: umbrella, M: manubrium, Ra: radial canal, Ri: ring canal, T: tentacle. (C) Tentacle of *Cladonema* medusa. O: ocellus, TB: tentacle bulb, Br: branch, NC: nematocyte cluster. (D) Tentacle regeneration processes after amputation while retaining the bulb. hpa: hour post-amputation. Yellow arrows indicate nematocyte clusters. n = 234/236 (tentacles). (E) Scheme of the tentacle regeneration that retains the bulb. (F) Distribution of mature nematocytes and localization of muscle fibers during tentacle regeneration. DAPI for poly-γ-glutamate (green) and nuclei (blue), and Phalloidin for F-actin (red). Yellow arrows indicate nematocyte clusters. (G) Neural morphology in the regenerating tentacle stained with the anti-FMRFamide antibody. Yellow arrows indicate neural fibers. (H) The regenerating tentacle is fully functional at 72 hpa. Image of the tentacle capturing prey, brine shrimp (White arrow). (I) The rate of functional tentacles across the regeneration time course. Intact: n = 40 (tentacles), 0-72 hpa: n = 36. (J) Tentacle regeneration process after removing the bulb from canals. Yellow arrow in (iv) indicates a nematocyte cluster. Dpa: day post-amputation. n = 117/219 (tentacles). Ra: radial canal, Ri: ring canal. (K) Scheme of tentacle regeneration without bulb. Scale bars: (B-D, J) 1 mm, (F, Gi) 100 μm, (Gii) 50 μm.

Fig 2. Blastema formation at early phase of tentacle regeneration. (A) Distribution of S-phase cells in intact and regenerating tentacle stained with EdU 1 h pulse labeling at intact as well as 24, 48, and 72 hpa, as shown in the scheme (A'). The tentacles were divided into three parts defined as basal (grey arrows), middle (pink arrows), and distal (red arrows). (B) Quantification of EdU^+ cells' distribution in regenerating tentacle based on the defined areas in (A). Intact: n = 19 (tentacles), 24 hpa: n = 10, 48 hpa: n = 9, 72 hpa: n = 8. (C) Scheme of proliferative cells distribution during tentacle regeneration. (D) Distribution of S-phase and M-phase cells stained with EdU 1 h pulse labeling

1211 and anti-Phospho-Histone 3 (PH3) antibody. EdU (green) and PH3 (magenta).
1212 Yellow dot squares show each quantification area (74.72^2 μm^2) in (E, F). (E, F)
1213 The proportion of $PH3^+$ and EdU^+ cells per all cells in each area. The regions of
1214 bulb (a) and amputation (amp) site were defined in intact tentacles while those
1215 of bulb (b) and blastema were defined in the regenerating tentacle at 24 hpa.
1216 Each area: n = 14. (G-I) Distribution of proliferative cells at 24 hpa: (G) After the
1217 distal side of tentacle is amputated, (H) after removing the bulb from canals,
1218 and (I) in isolated tentacles at 24 hpa. EdU 1 h pulse labeling at 24 hpa.
1219 Unpaired two-tailed *t*-test. *$p < 0.05$, **$p < 0.005$, ***$p < 0.001$. Scale bars: (A,
1220 G-I) 100 μm, (D) 50 μm.
1221
1222 **Fig 3. Stem cells and progenitor cells in blastema.**
1223 (A) Identification of cell types in blastema stained with anti-β-catenin staining.
1224 White arrow: epithelial cell, white arrow head: i-cell, yellow arrow head:
1225 nematocyte. Yellow dot square (ii) shows quantification area (35.10^2 μm^2) in
1226 (B). Magnified images for each cell type (iii). (B) Cell types in blastema at 24
1227 hpa by anti-β-catenin staining. n = 3 (areas). (C) FISH images of *Nanos1* gene
1228 expression from the proximal, abaxial side of the tentacle. Distribution of stem
1229 (*Nanos1*$^+$) cells in intact and regenerating tentacle. The tentacles were divided
1230 into three parts defined as basal (grey arrows), middle (pink arrows), and distal
1231 (red arrows). Yellow arrow indicates main tentacle, and white arrow indicates
1232 new branch. (D) Quantification of *Nanos1*$^+$ cells distribution in tentacles based
1233 on the defined areas in (C). Intact: n = 5, 24 hpa: n = 4 (tentacles), 48 hpa: n =
1234 4, 72 hpa: n = 5. (E) Images of the intact and regenerating tentacle co-labeled
1235 with *Nanos1* FISH and EdU 1 h pulse labeling. EdU (green) and *Nanos1*
1236 (magenta). White squares show the quantification area (74.72^2 μm^2) in (3F and
1237 S4E). Yellow arrowheads indicate EdU^+ and *Nanos1*$^+$ cells. (F) The ratio of
1238 *Nanos1*$^+$ cells / EdU^+ cells in intact and regenerating tentacles. The averages of
1239 *Nanos1*$^+$ cells / EdU^+ cells, intact bulb: 69.7% (n = 18), blastema: 30.3% (n =
1240 22). Unpaired two-tailed *t*-test. *$p < 0.05$, **$p < 0.005$, ***$p < 0.001$. Scale bars:
1241 (Ai, C, Ei and Eiii) 50 μm, (Eii and Eiv) 25 μm, (Aii) 10 μm.
1242
1243 **Fig 4. Distinct proliferative cell populations during tentacle regeneration.**
1244 (A) Scheme of lineage-tracing experiments using EdU and BrdU in (B-D).
1245 Resident homeostatic stem cells (RHSCs) are labeled by EdU before
1246 amputation; repair-specific proliferative cells (RSPCs) are labeled by BrdU at 24

1247 hpa. (B) Distribution of EdU^+ and $BrdU^+$ cells during tentacle regeneration. EdU
1248 (green) and BrdU (red). (C) The magnified images of bulb and blastema in (Bi).
1249 White arrowheads indicate EdU^+ and $BrdU^+$ cells. (D) Quantification of
1250 $EdU^+/BrdU^+$ cells in (C). Each quantification area size is 74.72^2 μm^2. The ratio
1251 of $EdU^+/BrdU^+$ cells. bulb: n = 10, blastema: n = 22. (E) The number of RHSCs
1252 during regeneration. Intact: n = 20 (tentacles), 24 hpa: n = 19, 48 hpa: n = 20,
1253 72 hpa: n = 16. (F) The number of RSPCs during regeneration. 24 hpa: n = 12,
1254 48 hpa: n = 12, 72 hpa: n = 6. For (E) and (F), quantification area is the whole
1255 regenerating tentacle. (G) Scheme of two proliferative cell populations during
1256 regeneration. (H) Scheme of stem cell elimination by X-ray irradiation (75 Gy) or
1257 drug treatments (HU 10 mM and Mitomycin C 30 μM) followed by labeling
1258 blastema with EdU (I-J). Tentacle amputation at 3 days post-irradiation/after
1259 treatment of drugs. (I) Distribution of proliferative cells after X-ray irradiation or
1260 drug treatments. EdU 1 h pulse labeling at 24 hpa. Yellow dot squares show
1261 each quantification area (74.72^2 μm^2) in (J). (J) The ratio of EdU^+ cells in
1262 blastema. Control: n = 12, X-ray: n = 13, HU: n = 12, Mitomycin C: n = 20.
1263 Unpaired two-tailed *t*-test. *$p < 0.05$, **$p < 0.005$, ***$p < 0.001$. Scale bars: (B, I)
1264 100 μm, (C) 20 μm.
1265
1266 **Fig 5. Contribution of resident homeostatic stem cells to nematogenesis**
1267 **and tentacle elongation.**
1268 (A) Scheme of EdU long-time (24 hours) and BrdU double chasing experiment
1269 in (B-C). (B) The distributions of EdU^+ and $BrdU^+$ cells during tentacle
1270 regeneration. EdU (green) and BrdU (red). Yellow arrows indicate accumulation
1271 of EdU^+ cells at nematocyte clusters in distal side at 72 hpa. White arrowheads
1272 indicate $EdU^+/BrdU^+$ cells. Yellow dot squares show magnified views (iv, v). (C)
1273 Quantification of $EdU^+/BrdU^+$ cells (%) in the blastema region (Biv). The
1274 quantification area is 74.72^2 μm^2. n = 29. (D) Cell type identification by anti-
1275 aPKC staining. i-cells, nematocytes, and epithelial cells, similar to the anti-β-
1276 catenin staining (see Fig 3A). (E) Scheme of experiments (F-G). RHSCs are
1277 labeled by EdU 24 hours incorporation before amputation and anti-aPKC
1278 staining at 72 hpa. (F) Cell type identification of EdU labeled cells in distal side
1279 at 72 hpa by anti-aPKC staining. EdU (green) and aPKC (magenta). White
1280 arrowheads show nematocytes. (G) Quantification of the cell types of EdU^+ cells
1281 on the distal side of a regenerating tentacle at 72 hpa. Quantification area of
1282 regenerating tentacle is 74.72^2 μm^2. n = 10. (H) Experimental scheme for

1283 tentacle regeneration after X-ray irradiation (75 Gy) or drug treatments (HU 10
1284 mM and Mitomycin C 30 μM) in (I-K). Tentacle amputation at 3 days post-
1285 irradiation or after 3 days treatment of drugs. (I) Representative images of
1286 regenerating tentacles at 3 dpa. Yellow arrowheads indicate nematocyte
1287 clusters. (J) The timing of nematocyte cluster formation in regenerating
1288 tentacles. Control: n = 48, HU: n = 51, Mitomycin C: n = 51, X-ray: n = 60. (K)
1289 Length of regenerating tentacle after irradiation and drug treatments. Control: n
1290 = 48, HU: n = 51, Mitomycin C: n = 51, X-ray: n = 60. Unpaired two-tailed *t*-test.
1291 *$p < 0.05$, **$p < 0.005$, ***$p < 0.001$. Scale bars: (I) 1 mm, (Bi-iii) 100 μm, (Biv
1292 and Bv) 50 μm, (F) 25 μm.
1293
1294 **Fig 6. Contribution of repair-specific proliferative cells to tentacle**
1295 **elongation.**
1296 (A) Experimental scheme for combining the identification of cell types by anti-
1297 aPKC staining and EdU chasing in (B-C). (B) Identification of cell types of EdU^+
1298 cells in blastema at 24 hpa and the distal side of the regenerating tentacle at 72
1299 hpa by anti-aPKC staining. EdU (green) and aPKC (magenta). White arrow:
1300 epithelial cell, white arrow head: i-cell. Magnified views (iii, iv). (C) Quantification
1301 of cell types in EdU^+ cells at 24 and 72 hpa. Quantification area of regenerating
1302 tentacle is 35.06^2 μm^2. 24 hpa: n = 9, 72 hpa: n = 12. (D) Experimental scheme
1303 depicting blastema monitoring after UV exposure in (E-F). EdU 1 h
1304 incorporation at 24 hpa and UV exposure around the blastema region. (E)
1305 Distribution of EdU labeled cells during regeneration, Ctl (no UV) vs UV. (F) The
1306 number of EdU^+ cells from 24 hpa to 72 hpa, Ctl (no UV) vs UV. 24 hpa: n = 11
1307 (tentacles), 48 hpa Ctl: n = 18, 48 hpa UV: n = 20, 72 hpa Ctl: n = 10, 72 hpa
1308 UV: n = 10. (G) Experimental scheme for measuring of regenerating tentacle
1309 after UV exposure to blastema at 24 hpa (H & I). (H) Representative images of
1310 regenerating tentacles at 96 hpa. (I) Length of the regenerating tentacle after
1311 UV exposure on blastema. Ctl: n = 12 (tentacles), UV: n = 12. Unpaired two-
1312 tailed *t*-test. *$p < 0.05$, **$p < 0.005$, ***$p < 0.001$. Scale bars: (H) 1 mm, (E) 100
1313 μm, (Bi and Bii) 50 μm, (Biii and Biv) 10 μm.
1314
1315 **Fig 7. Summary of *Cladonema* tentacle regeneration and evolutionary**
1316 **history of appendage regeneration.**
1317 (A) When a *Cladonema* medusa tentacle is amputated, wound closure is
1318 completed by 24 hpa. After wound healing, repair-specific proliferative cells

1319 (RSPCs) appear and actively proliferate at the wound tip. Ectopic cell
1320 proliferation on the distal side is gradually suppressed, and the cell
1321 differentiation phase begins. While resident homeostatic stem cells (RHSCs) in
1322 the bulb supply nematocytes and epithelial cells, RSPCs mainly differentiate
1323 into epithelial cells. (B) Blastema formation mechanism during appendage
1324 regeneration across animal evolution. When an appendage is amputated,
1325 RSPCs (stem/progenitor cells) contribute to blastema formation in both
1326 regenerative bilaterians (e.g. salamanders) and cnidarian jellyfish.
1327
1328 **Supplementary Figures**
1329 **Fig S1. Wound healing, neuron regeneration and the rate of regeneration.**
1330 (A) Representative images of nematocyte clusters (NC) in the medusa tentacle.
1331 Yellow arrows indicate nematocyte clusters that include mature nematocytes
1332 (Poly-γ-glutamate^{+}). (B) The process of wound healing from 4 hpa to 24 hpa
1333 with Phalloidin and anti-α-Tubulin antibody. Phalloidin for F-actin (red) and α-
1334 Tubulin (green). (C) The extent of wound healing during tentacle regeneration.
1335 Full open: actin fibers not attached (Bi), Partially close: disorganized actin fibers
1336 (Bii and Biii), Completed close: actin fibers are fully attached (Biv). 4 hpa: n = 15
1337 (tentacles), 8 hpa: n = 17, 16 hpa: n = 15, 24 hpa: n = 14. (D) Neural
1338 morphology in intact tentacle and the regenerating tentacle stained with the
1339 anti-FMRFamide antibody. Yellow allows indicate cell bodies of FMRFamide
1340 neurons. FMRFamide (magenta). (i, ii) Intact whole tentacle, (iii, iv) basal side of
1341 intact tentacle, (v, vi) regenerating tentacle at 24 hpa. (E) Neural morphology in
1342 the regenerating tentacle stained with the anti-acetylated-Tubulin antibody.
1343 White arrows indicate neural fibers. acetylated-Tubulin (green). (F) The rate of
1344 the tentacle regeneration after removing the bulb from canals. Difference of the
1345 regeneration rate between each experiment. (G) Images of the isolated tentacle
1346 without bulb at 1 dpa and 7 dpa. (H) Images of the isolated whole tentacle 1 dpa
1347 and 7 dpa. Scale bars: (A, Di, Diii, Dv and Ei, Eiii) 100 μm, (Div, Dvi and Eii, Eiv)
1348 50 μm, (G, H) 1 mm.
1349
1350 **Fig S2. The distribution of mitotic cells during regeneration.**
1351 (A) Distribution of mitotic cells detected by anti-PH3 in regenerating tentacle. (B)
1352 Quantification of PH3^{+} cells' distribution in regenerating tentacle based on the
1353 defined areas in (A). Intact: n = 11 (tentacles), 24 hpa: n = 10, 48 hpa: n = 9, 72
1354 hpa: n = 8. (C) Distribution of S-phase cells in regenerating tentacle stained with

1355 EdU 1 h pulse labeling. EdU 1h pulse labeling was performed at 0, 4, 8, 12, 16,
1356 20, and 24 hpa as shown in the scheme. White dot squares show each
1357 quantification area (150^2 μm^2) in (D, E). (D) EdU relative intensity in blastema. 0
1358 hpa: n = 6, 4 hpa: n = 7, 8 hpa: n = 10, 12 hpa: n = 11, 16 hpa: n = 10, 20 hpa:
1359 n = 26, 24 hpa: n = 12. (E) The number of EdU^+ cells in blastema. 0 hpa: n = 6,
1360 4 hpa: n = 7, 8 hpa: n = 10, 12 hpa: n = 11, 16 hpa: n = 10, 20 hpa: n = 26, 24
1361 hpa: n = 12. Scale bars: (A, C) 100 μm.
1362
1363 **Fig S3. The distribution of stem cells in intact tentacle.**
1364 (A-D) Expression of *Nanos1, Nanos2, Piwi,* and *Vasa1* in intact tentacles by
1365 FISH. Yellow arrows indicate the branching site. (E) Expression of *Nanos1* and
1366 *Nanos2* in intact tentacle by double FISH. White arrowheads indicate *Nanos1*$^+$*,*
1367 and white arrows indicate *Nanos2*$^+$. (F) Expression of *Nanos2* and *Mcol1* in
1368 intact tentacle by double FISH. Yellow arrows indicate representative co-
1369 expression of *Nanos2* and *Mcol1*. Scale bars: (A-D) 100 μm, (Ei, Fi) 50 μm, (Eii,
1370 Fii) 25 μm.
1371
1372 **Fig S4. The distribution of stem-like cells in regenerating tentacle.**
1373 (A, B) Distribution of cells with stem marker genes (*Piwi*$^+$ or *Vasa1*$^+$) in intact
1374 tentacle and regenerating tentacle by FISH. Yellow arrow indicates the
1375 branching site. (C, D) Images of the regenerating tentacle co-labeled with *Piwi*
1376 or *Vasa1* FISH and EdU 1 h pulse labeling at 24 hpa. EdU (green) and *Piwi* or
1377 *Vasa1* (magenta). White squares show each quantification area (74.72^2 μm^2) in
1378 (E). Yellow arrowheads indicate EdU^+/*Piwi*$^+$ or EdU^+/*Vasa1*$^+$ cell. (E) The rate of
1379 cells positive for stem cell marker genes in blastema. *Nanos1*: n = 22, *Piwi*: n =
1380 12, *Vasa1*: n = 11. Scale bars: (Aiv, Biv) 100 μm, (Ai-iii, Bi-iii, Ci and Di) 50 μm,
1381 (Cii and Dii) 25 μm.
1382
1383 **Fig S5. Distribution and increase of resident homeostatic stem cells**
1384 **(RHSCs) during tentacle regeneration.**
1385 (A) Transition of labeled RHSCs during regeneration by chasing EdU^+ cells.
1386 EdU 1 h labeling before amputation and chasing at 0, 4, 8, 12, 16, 24, 48, 72
1387 hpa. White dot squares show each quantification area (150^2 μm^2) in (B). (B) The
1388 number of EdU^+ cells around blastema during regeneration. 0 hpa: n = 6, 4 hpa:
1389 n = 6, 8 hpa: n = 13, 12 hpa: n = 12, 16 hpa: n = 8, 24 hpa: n = 10. (C) The
1390 comparison of proliferative cell number in intact vs no amputation vs 24 hpa.

1391 EdU 1 h pulse labeling before amputation and chasing with amputation or
1392 without amputation (no amp). (D) The number of EdU^+ cells labeled before
1393 amputation. Counted area is the whole regenerating tentacle at 24 hpa.
1394 Detailed information is in (E). Intact: n = 6 (tentacles), 24 h (no amp): n = 6, 24
1395 hpa: n = 6. (E) Area size used for quantification. Note that the area of
1396 quantification at 24 hpa is similar. Unpaired two-tailed *t*-test. $*p < 0.05$, $**p <$
1397 0.005, $***p < 0.001$. Scale bars: (A, C) 100 μm.
1398
1399 **Fig S6. DiI injection revealed that resident stem cells do not migrate to**
1400 **blastema during regeneration.**
1401 (A) Experimental scheme of DiI labeled cell identification in the bulb with EdU or
1402 anti-β-catenin staining in (B). (B) Co-staining of DiI and EdU or anti-β-catenin in
1403 intact tentacle. White dot squares show each quantification area (74.72^2 μm^2) in
1404 (C). (C) Rate of DiI labeled cells per proliferative cells or i-cells in bulb.
1405 Quantification of DiI^+/EdU^+ cells or DiI^+/i-cells (β-catenin cytoplasmic signal$^+$
1406 cells). DiI^+/EdU^+ cells: n = 5 (areas), DiI^+/i-cells: n = 5. (D) Experimental scheme
1407 of chasing DiI-labeled cells in (E). EdU 1h pulse labeling at 24 hpa. (E) (i and ii)
1408 Little migration of DiI labeled cells in bulb from the moment of amputation to 24
1409 hpa. n = 9/9. (iii and iv) DiI labeled cells in center area that merged with EdU
1410 (yellow arrow). n = 10/12. (F) Experimental scheme for chasing DiI-labeled cells
1411 in the bulb in (G). (G) Distribution change of DiI labeled cells in the bulb during
1412 tentacle regeneration of an animal. White arrow indicates migration of labeled
1413 cells to nematocyte cluster at distal side. n = 6/10. (H) Experimental scheme for
1414 chasing DiI-labeled cells in the central area of tentacle in (I). (I) Distribution
1415 change of DiI-labeled cells in central area during tentacle regeneration of an
1416 animal. White arrow indicates DiI-labeled cells in the newly regenerated
1417 tentacle. n = 17/19. Scale bars: (G, I) 250 μm, (Bi, Biii, E) 100 μm, (Bii, Biv) 50
1418 μm.
1419
1420 **Fig S7. *Nanos1*$^+$ cells in the bulb decrease after X-ray irradiation or drug**
1421 **treatments.**
1422 (A) Experimental scheme of X-ray irradiation (30, 50, 75 Gy). FISH and qPCR
1423 at 3 days post-irradiation (3 dpi). (B) Expression of *Nanos1* in intact tentacle at
1424 3 dpi by FISH. (C) Quantification of *Nanos1*$^+$ cells number in tentacle.
1425 Quantification area is the entire tentacle in confocal images. Control: n = 9, 30
1426 Gy: n = 5, 50 Gy: n = 5, 75 Gy: n = 17. (D) Experimental scheme of drug

1427 treatments (HU 10 mM or Mitomycin C 30 μM). FISH and qPCR after 3 days of
1428 treatment. (E) Expression of *Nanos1* in intact tentacle after 3 days drug
1429 treatments by FISH. (F) Quantification of *Nanos1*$^+$ cells in tentacle.
1430 Quantification area is the entire tentacle in confocal images. Control: n = 9, 75
1431 Gy: n = 17, HU: n = 10, Mitomycin C: n = 8. (G) Relative expression of *Nanos1*
1432 after irradiation and drug treatments by qPCR. Unpaired two-tailed *t*-test. *p <
1433 0.05, **p < 0.005, ***p < 0.001. Scale bars: (B, E) 50 μm.
1434
1435 **Fig S8. EdU long incorporation labels nematocyte progenitors.**
1436 (A) Nematocyte progenitor cells in the bulb with dual staining of *Mcol1* FISH and
1437 EdU staining. EdU 1 h or 24 h pulse labeling. The expression level of *Mcol1* is
1438 extremely high such that the *Mcol1* signal invades the wavelength of the EdU
1439 signal. White arrows indicate EdU$^+$ cells, and yellow arrowheads indicate
1440 *Mcol1*$^+$/EdU$^+$ cells. (B) The rate of *Mcol1*/EdU$^+$ cells in intact tentacle.
1441 Quantification area is the entire tentacle in single section of confocal images. 1
1442 h: n = 7 (tentacles), 24 h: n = 7. Unpaired two-tailed *t*-test. **p < 0.005. Scale
1443 bars: (A) 50 μm.
1444
1445 **Fig S9. Similar pattern between β-catenin and aPKC antibody staining.**
1446 Identification of cell types in blastema stained by β-catenin and aPKC antibody
1447 staining. Scale bar: 50 μm.
1448
1449 **Fig S10. Neurons are newly-generated from two stem-like cell populations**
1450 **during regeneration.**
1451 (A) Experimental scheme of chasing RHSCs in (B). (B) Neuron derived from
1452 RHSCs by co-staining with EdU and anti-FMRFamide antibody at 72 hpa.
1453 Yellow arrowhead indicates EdU$^+$ & FMRFamide$^+$ cell. (C) Experimental scheme
1454 of chasing RSPCs in (D). (D) Neuron derived from RSPCs by co-staining wtih
1455 EdU and anti-FMRFamide antibody at 72 hpa. Yellow arrowhead indicates
1456 EdU$^+$ & FMRFamide$^+$ cell. (E) (i) The number of neurons in each chasing
1457 experiment. Quantification area is the entire tentacle in confocal images (B ii
1458 and D ii). RSPCs: n = 19 (images), RHSCs: n = 18. (ii) Rate of
1459 EdU$^+$/FMRFamide$^+$ cell in (Ei). Unpaired two-tailed *t*-test. *p < 0.05. Scale bars:
1460 (Bi, Di) 100 μm, (Bii, Dii) 50 μm.
1461
1462 **Fig S11. Blastema exposure to UV has no significant effect on RHSCs.**

1463 (A) Experimental scheme depicting the combination of EdU chasing and UV
1464 exposure in (B-D). (B) Bleaching of Hoechst signal only in UV exposure area at
1465 24 hpa. White dot square is UV exposure area. (C) Distribution of EdU labeled
1466 cells from intact to 72 hpa, Ctl (no UV) vs UV. (D) The number of EdU^+ cells
1467 during regeneration, Ctl (no UV) vs UV. 24 hpa: n = 11 (tentacles), 48 hpa Ctl: n
1468 = 18, 48 hpa UV: n = 20, 72 hpa Ctl: n = 10, 72 hpa UV: n = 10. (E)
1469 Experimental scheme depicting nematogenesis monitoring after UV exposure in
1470 (F-G). (F) Representative images of Ctl vs UV at 72 hpa. Yellow arrowheads
1471 show nematocyte clusters. (G) Timing of nematocyte cluster formation during
1472 tentacle regeneration, Ctl vs UV. Each tentacle: n = 12. Unpaired two-tailed *t*-
1473 test. ***$p < 0.001$. Scale bars: (F) 500 μm, (B, C) 100 μm.
1474
1475

Figure 1

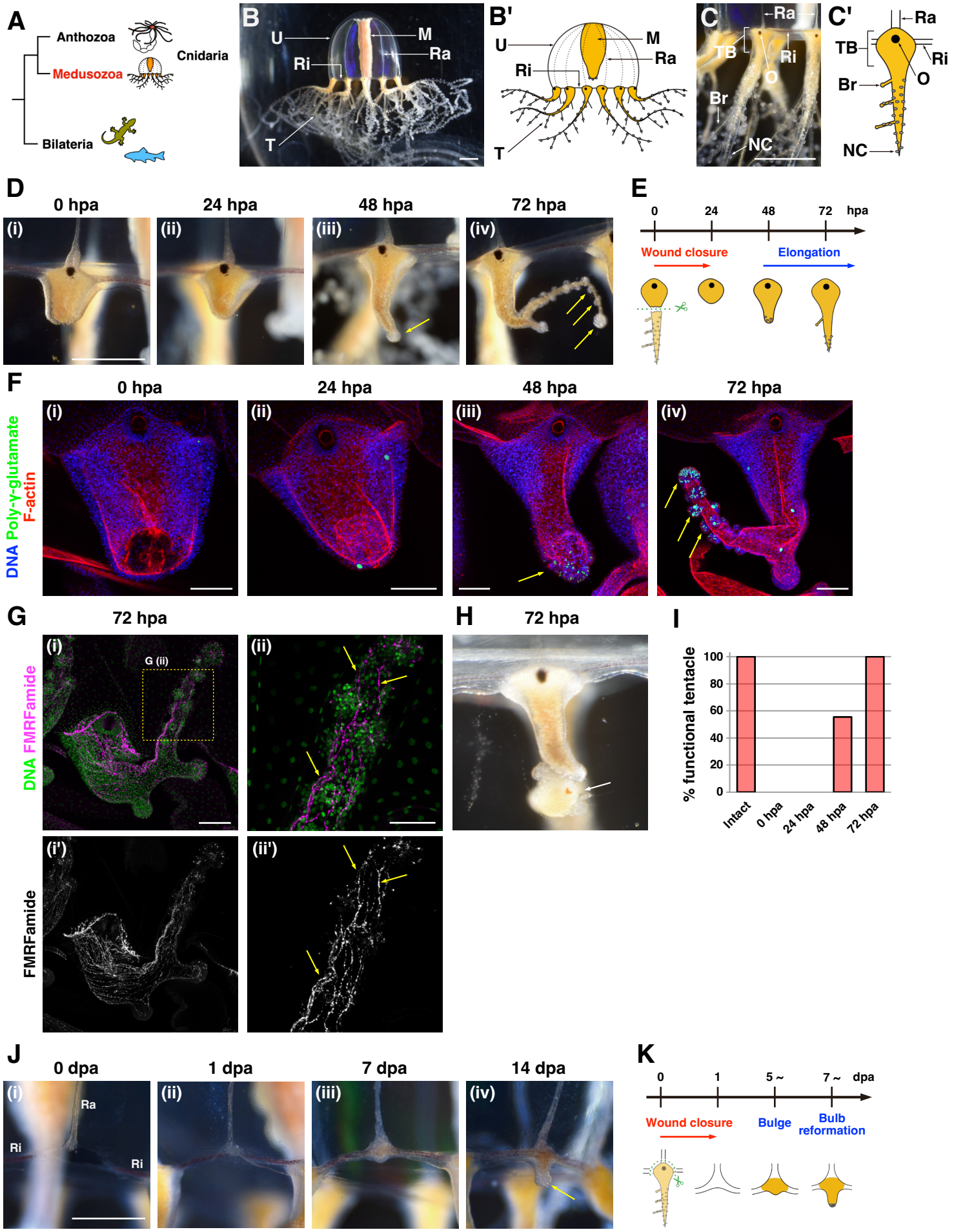
A
Anthozoa
Medusozoa
Cnidaria
Bilateria
B
U
M
Ri
Ra
T
B'
U
M
Ra
Ri
T
C
Ra
TB
Ri
O
Br
NC
C'
Ra
TB
Ri
Br
O
NC
D
0 hpa
24 hpa
48 hpa
72 hpa
(i)
(ii)
(iii)
(iv)
E
0
24
48
72
hpa
Wound closure
Elongation
F
0 hpa
24 hpa
48 hpa
72 hpa
DNA Poly-γ-glutamate
F-actin
(i)
(ii)
(iii)
(iv)
G
72 hpa
DNA FMRFamide
(i)
G (ii)
(ii)
FMRFamide
(i')
(ii')
H
72 hpa
I
% functional tentacle
100
80
60
40
20
0
Intact
0 hpa
24 hpa
48 hpa
72 hpa
J
0 dpa
1 dpa
7 dpa
14 dpa
(i)
Ra
Ri
Ri
(ii)
(iii)
(iv)
K
0
1
5 ~
7 ~
dpa
Wound closure
Bulge
Bulb reformation

Figure 2

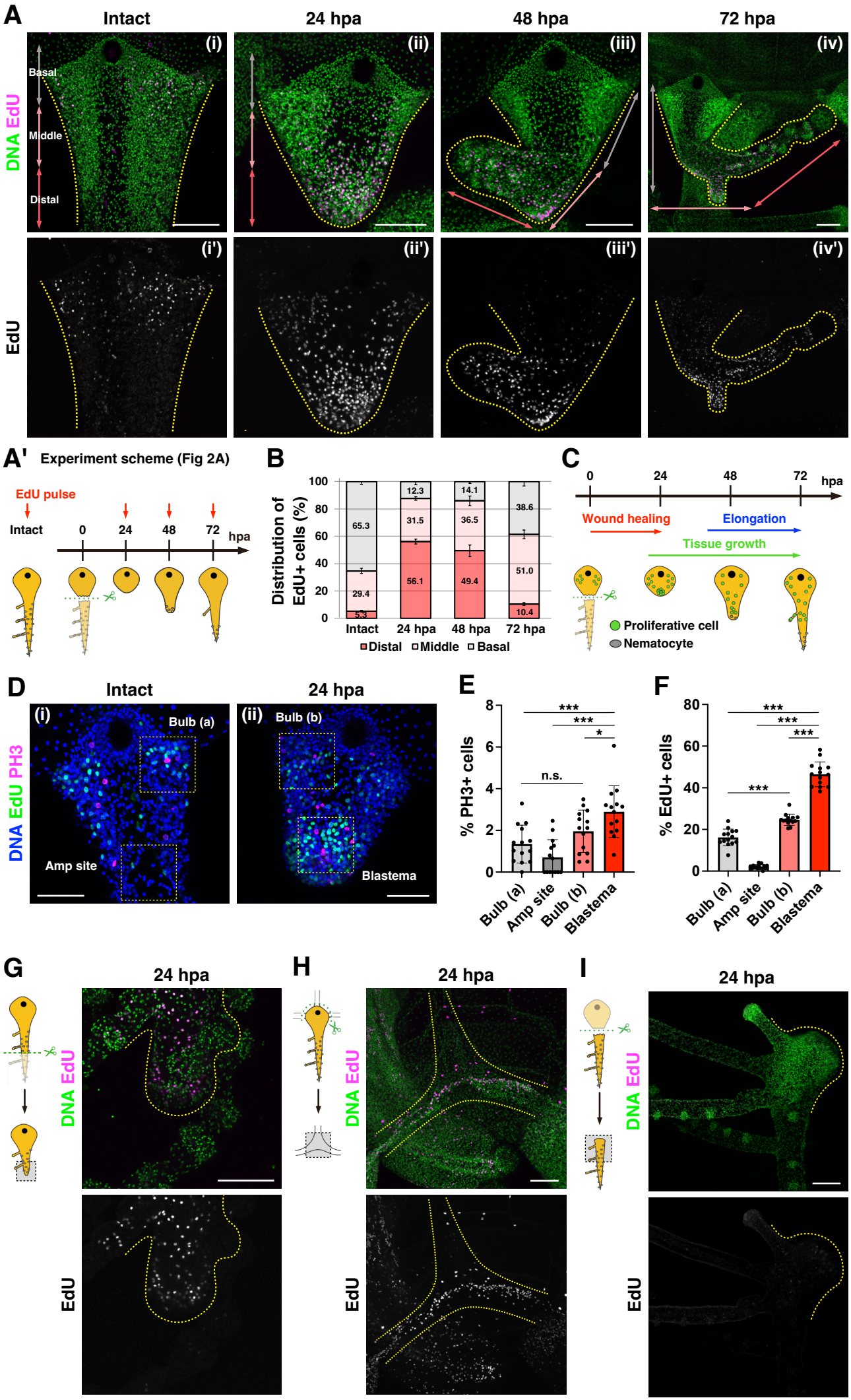
A
Intact
24 hpa
48 hpa
72 hpa
(i)
(ii)
(iii)
(iv)
Basal
Middle
Distal
DNA EdU
(i')
(ii')
(iii')
(iv')
EdU
A'
Experiment scheme (Fig 2A)
EdU pulse
Intact
0
24
48
72
hpa
B
Distribution of EdU+ cells (%)
100
80
60
40
20
0
65.3
29.4
5.3
12.3
31.5
56.1
14.1
36.5
49.4
38.6
51.0
10.4
Intact
24 hpa
48 hpa
72 hpa
Distal
Middle
Basal
C
0
24
48
72
hpa
Wound healing
Elongation
Tissue growth
Proliferative cell
Nematocyte
D
Intact
24 hpa
(i)
(ii)
Bulb (a)
Bulb (b)
Amp site
Blastema
DNA EdU PH3
E
% PH3+ cells
8
6
4
2
0
***
***
*
n.s.
Bulb (a)
Amp site
Bulb (b)
Blastema
F
% EdU+ cells
80
60
40
20
0
***
***
***
***
Bulb (a)
Amp site
Bulb (b)
Blastema
G
24 hpa
H
24 hpa
I
24 hpa
DNA EdU
EdU

Figure 3

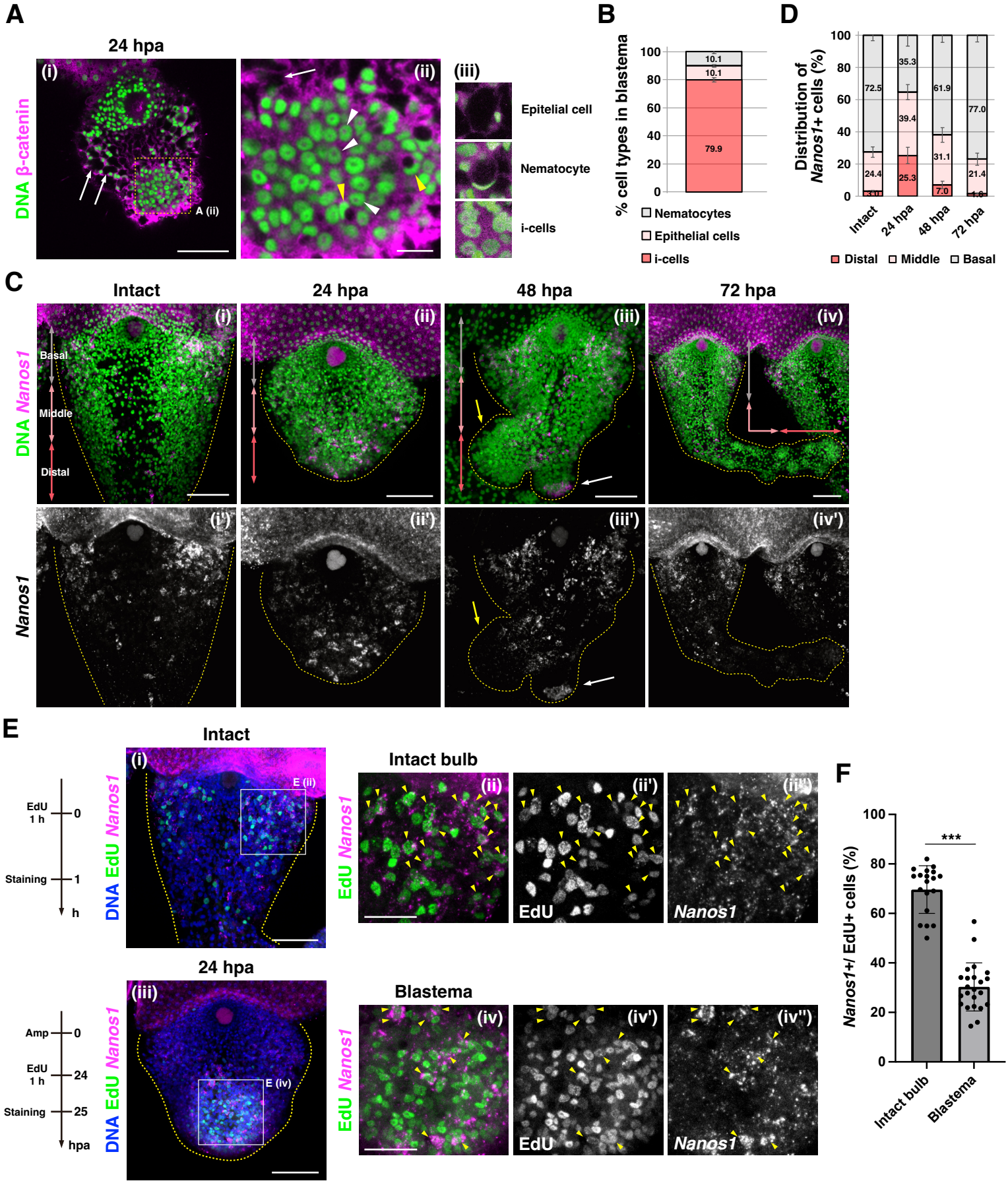
A
24 hpa
DNA β-catenin
(i)
(ii)
(iii)
A (ii)
Epitelial cell
Nematocyte
i-cells
B
% cell types in blastema
10.1
10.1
79.9
Nematocytes
Epithelial cells
i-cells
D
Distribution of Nanos1+ cells (%)
72.5
24.4
3.1
35.3
39.4
25.3
61.9
31.1
7.0
77.0
21.4
1.6
Intact
24 hpa
48 hpa
72 hpa
Distal
Middle
Basal
C
Intact
24 hpa
48 hpa
72 hpa
DNA Nanos1
Basal
Middle
Distal
Nanos1
E
Intact
EdU 1 h
Staining
DNA EdU Nanos1
E (ii)
Intact bulb
EdU Nanos1
EdU
Nanos1
24 hpa
Amp
EdU 1 h
Staining
hpa
E (iv)
Blastema
F
Nanos1+/ EdU+ cells (%)
***
Intact bulb
Blastema

Figure 4

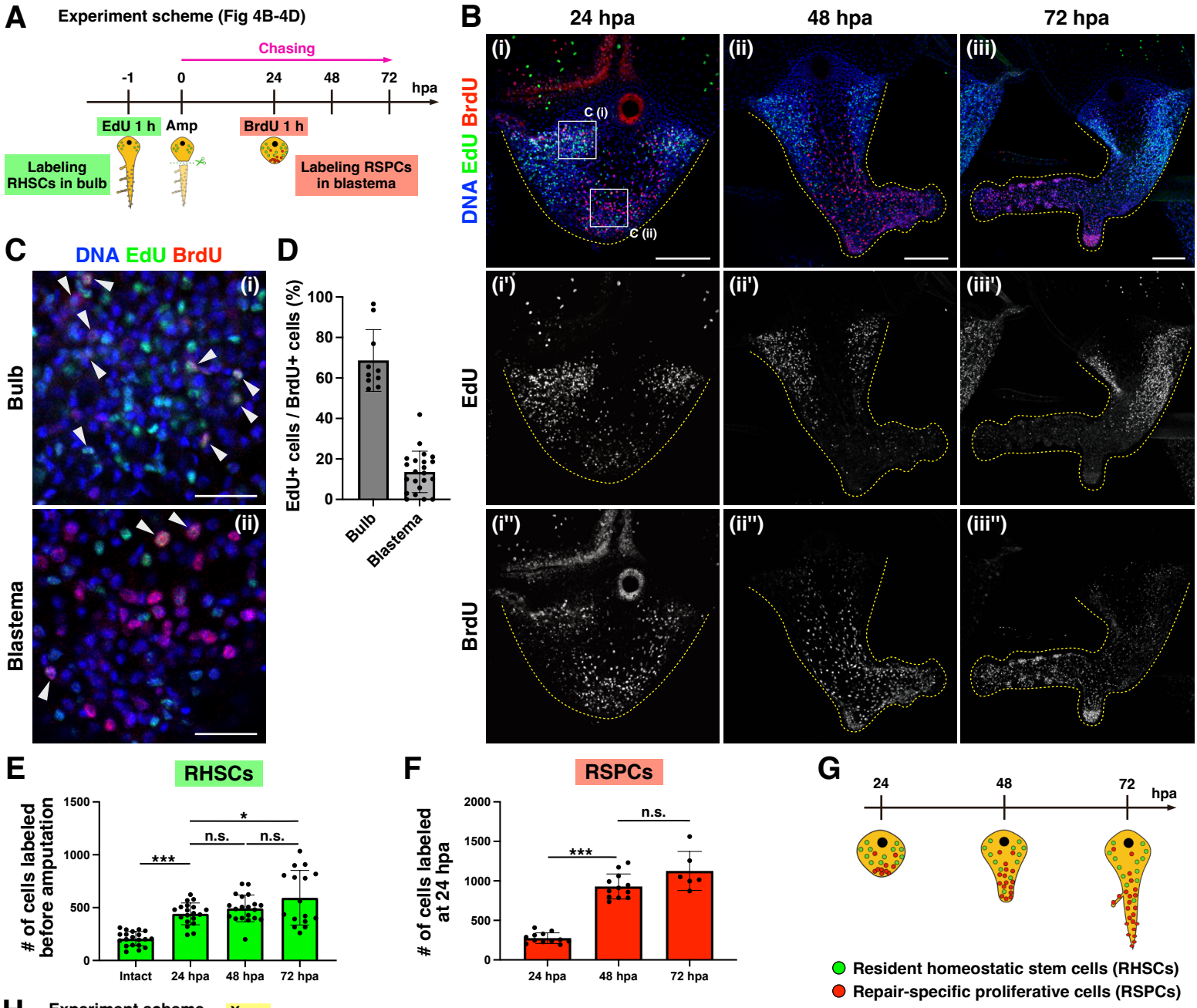
A
Experiment scheme (Fig 4B-4D)
Chasing
-1
0
24
48
72
hpa
EdU 1 h
Amp
BrdU 1 h
Labeling RHSCs in bulb
Labeling RSPCs in blastema
B
24 hpa
48 hpa
72 hpa
DNA EdU BrdU
(i)
(ii)
(iii)
C (i)
C (ii)
(i')
(ii')
(iii')
EdU
(i'')
(ii'')
(iii'')
BrdU
C
DNA EdU BrdU
Bulb
Blastema
(i)
(ii)
D
EdU+ cells / BrdU+ cells (%)
100
80
60
40
20
0
Bulb
Blastema

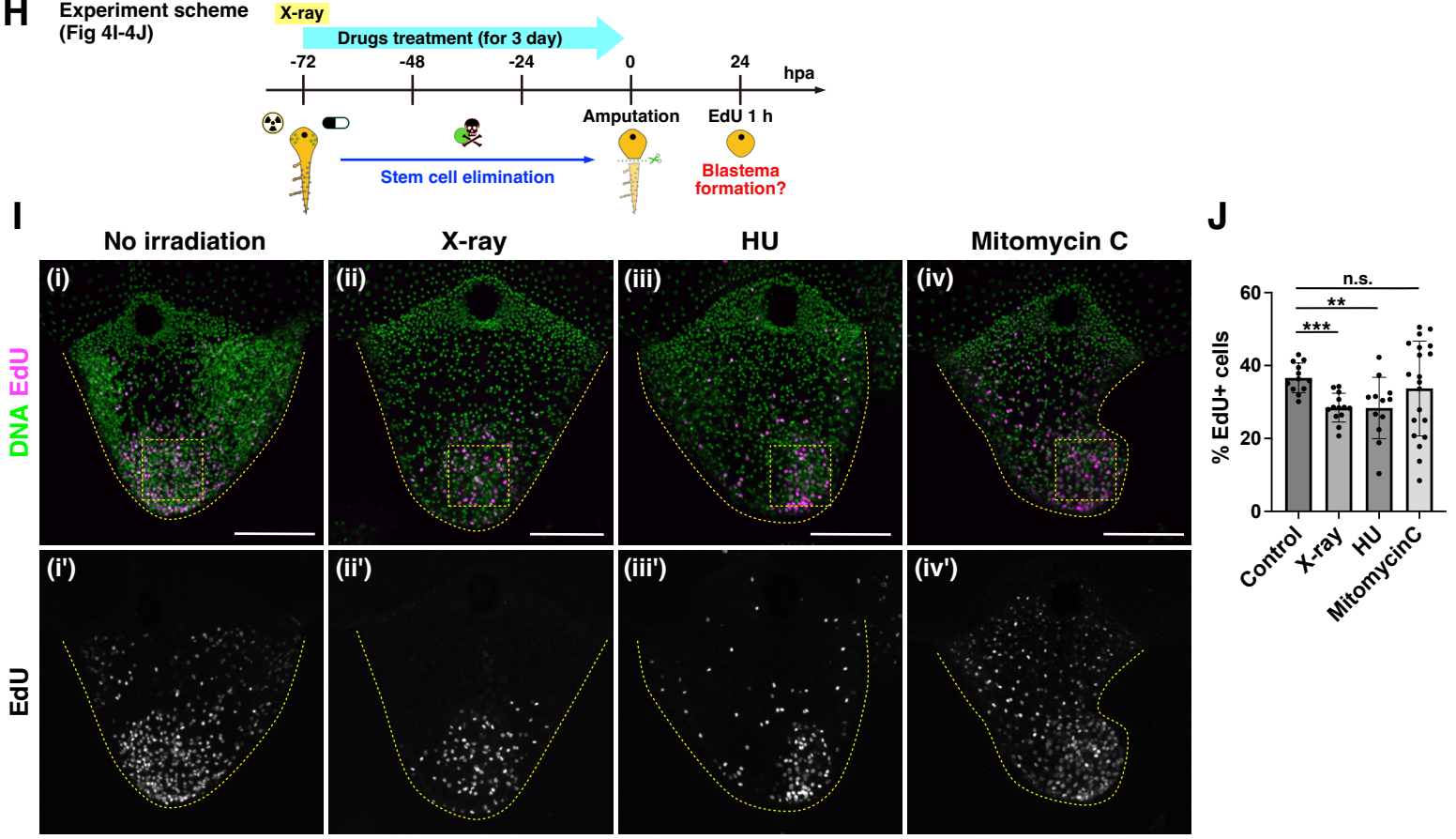
E
RHSCs
# of cells labeled before amputation
1500
1000
500
0
***
n.s.
n.s.
*
Intact
24 hpa
48 hpa
72 hpa
F
RSPCs
# of cells labeled at 24 hpa
2000
1500
1000
500
0
***
n.s.
24 hpa
48 hpa
72 hpa
G
24
48
72
hpa
Resident homeostatic stem cells (RHSCs)
Repair-specific proliferative cells (RSPCs)
H
Experiment scheme (Fig 4I-4J)
X-ray
Drugs treatment (for 3 day)
-72
-48
-24
0
24
hpa
Amputation
EdU 1 h
Stem cell elimination
Blastema formation?
I
No irradiation
X-ray
HU
Mitomycin C
DNA EdU
(i)
(ii)
(iii)
(iv)
(i')
(ii')
(iii')
(iv')
EdU
J
% EdU+ cells
60
40
20
0
n.s.
**
***
Control
X-ray
HU
MitomycinC

Figure 5

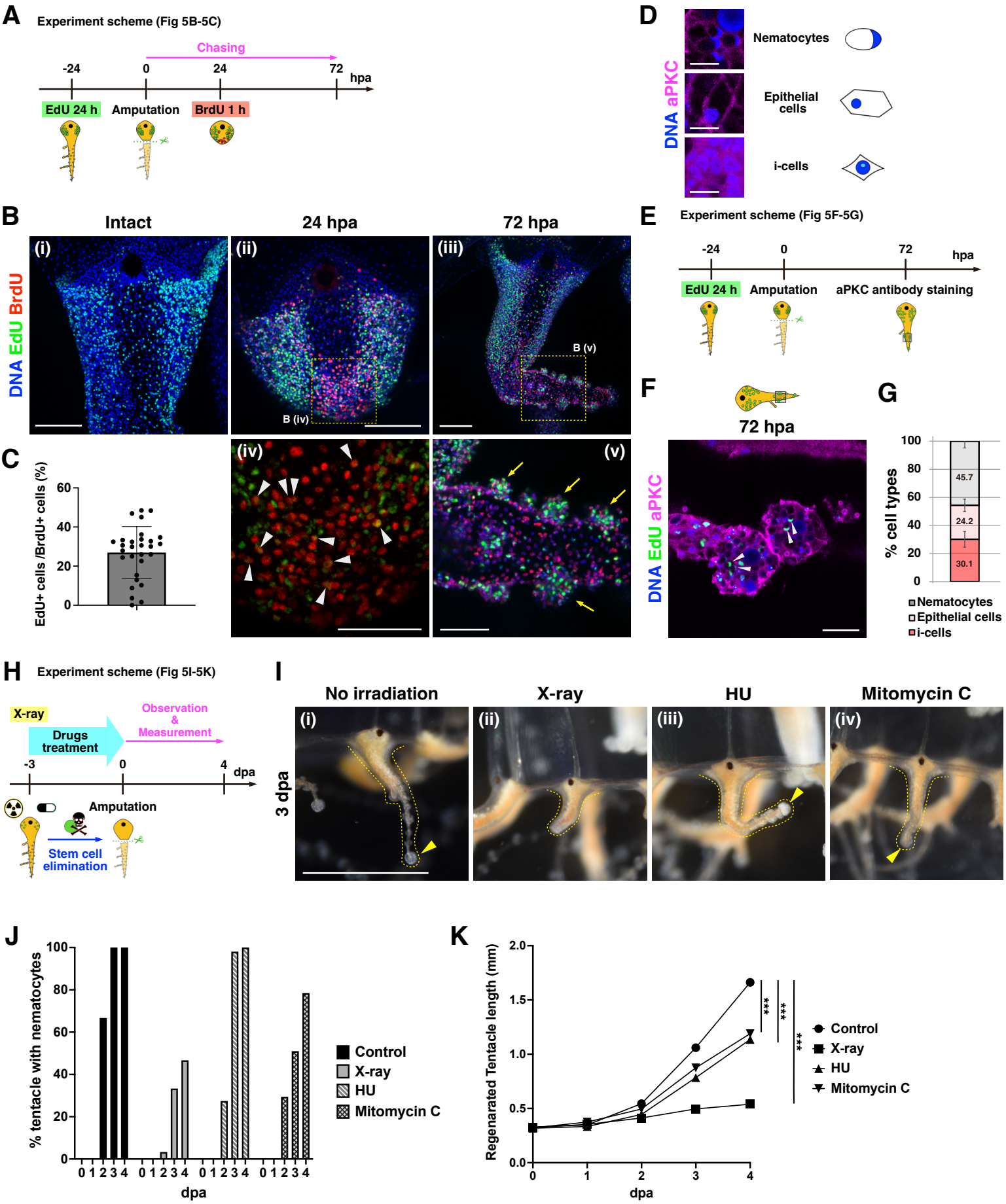
A
Experiment scheme (Fig 5B-5C)
Chasing
-24
0
24
72
hpa
EdU 24 h
Amputation
BrdU 1 h
B
Intact
24 hpa
72 hpa
DNA EdU BrdU
(i)
(ii)
(iii)
B (iv)
B (v)
(iv)
(v)
C
EdU+ cells /BrdU+ cells (%)
60
40
20
0
D
DNA aPKC
Nematocytes
Epithelial cells
i-cells
E
Experiment scheme (Fig 5F-5G)
-24
0
72
hpa
EdU 24 h
Amputation
aPKC antibody staining
F
72 hpa
DNA EdU aPKC
G
% cell types
100
80
60
40
20
0
45.7
24.2
30.1
Nematocytes
Epithelial cells
i-cells
H
Experiment scheme (Fig 5I-5K)
X-ray
Drugs treatment
Observation & Measurement
-3
0
4
dpa
Amputation
Stem cell elimination
I
No irradiation
X-ray
HU
Mitomycin C
3 dpa
(i)
(ii)
(iii)
(iv)
J
% tentacle with nematocytes
100
80
60
40
20
0
0 1 2 3 4 0 1 2 3 4 0 1 2 3 4 0 1 2 3 4
dpa
Control
X-ray
HU
Mitomycin C
K
Regenarated Tentacle length (mm)
2.0
1.5
1.0
0.5
0.0
0
1
2
3
4
dpa
***
***
***
Control
X-ray
HU
Mitomycin C

Figure 6

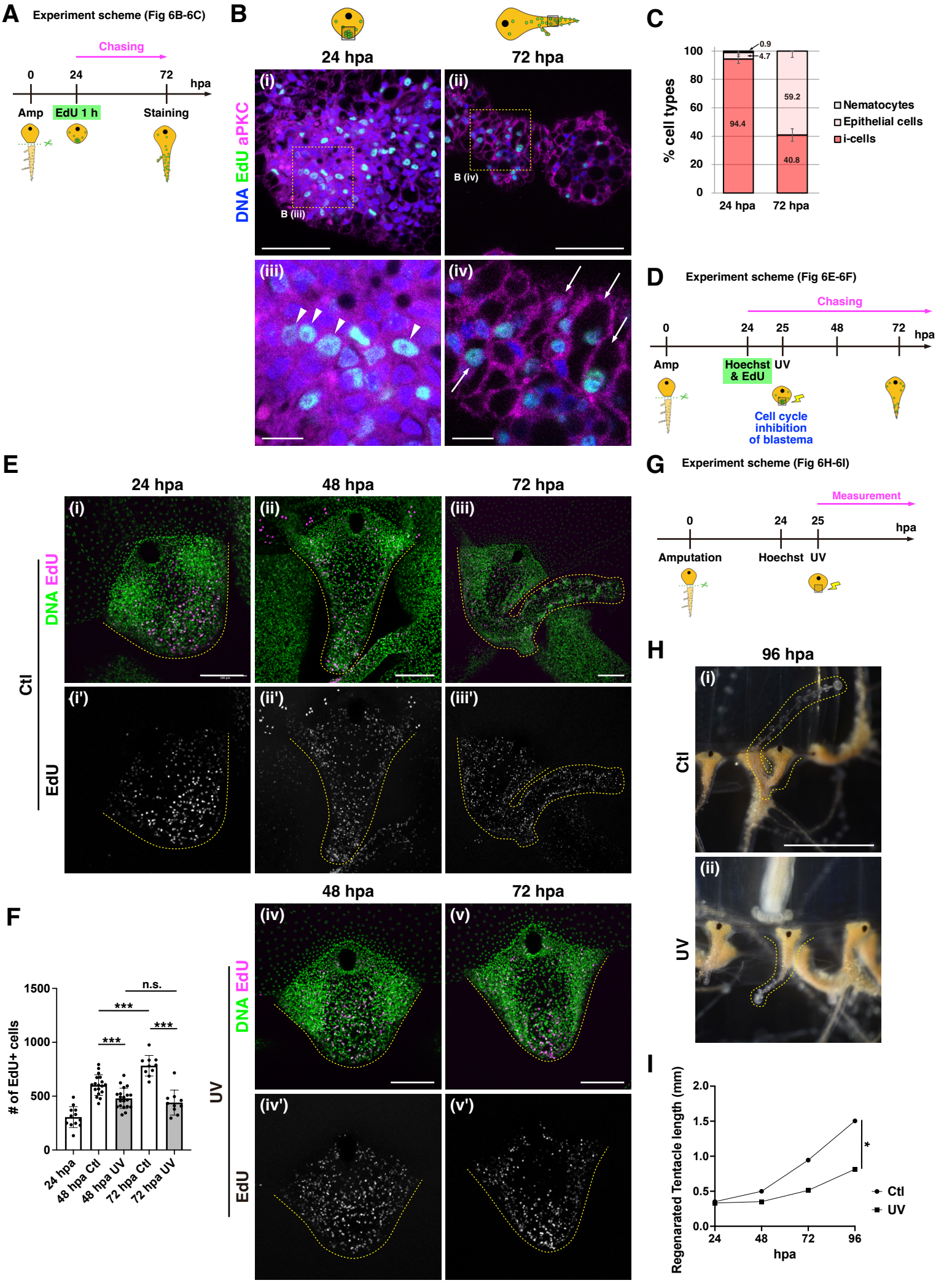
A
Experiment scheme (Fig 6B-6C)
Chasing
0
24
72
hpa
Amp
EdU 1 h
Staining
B
24 hpa
72 hpa
DNA EdU aPKC
(i)
(ii)
(iii)
(iv)
B (iii)
B (iv)
C
% cell types
100
80
60
40
20
0
0.9
4.7
94.4
59.2
40.8
24 hpa
72 hpa
Nematocytes
Epithelial cells
i-cells
D
Experiment scheme (Fig 6E-6F)
Chasing
0
24
25
48
72
hpa
Amp
Hoechst & EdU
UV
Cell cycle inhibition of blastema
E
24 hpa
48 hpa
72 hpa
Ctl
DNA EdU
EdU
(i)
(ii)
(iii)
(i')
(ii')
(iii')
F
# of EdU+ cells
1500
1000
500
0
n.s.
***
***
***
24 hpa
48 hpa Ctl
48 hpa UV
72 hpa Ctl
72 hpa UV
UV
DNA EdU
EdU
48 hpa
72 hpa
(iv)
(v)
(iv')
(v')
G
Experiment scheme (Fig 6H-6I)
Measurement
0
24
25
hpa
Amputation
Hoechst
UV
H
96 hpa
Ctl
UV
(i)
(ii)
I
Regenarated Tentacle length (mm)
2.0
1.5
1.0
0.5
0.0
24
48
72
96
hpa
*
Ctl
UV

Figure 7

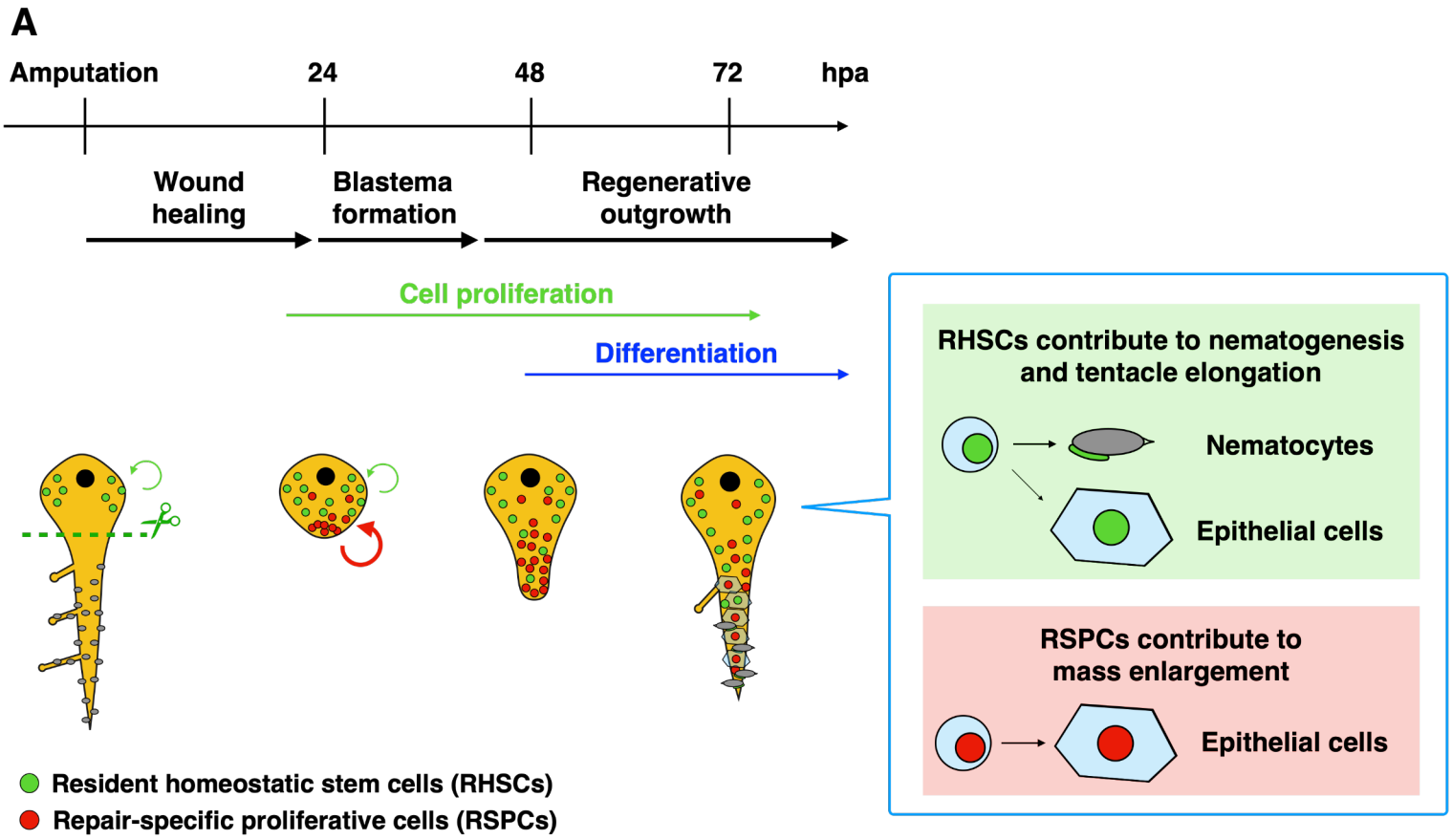
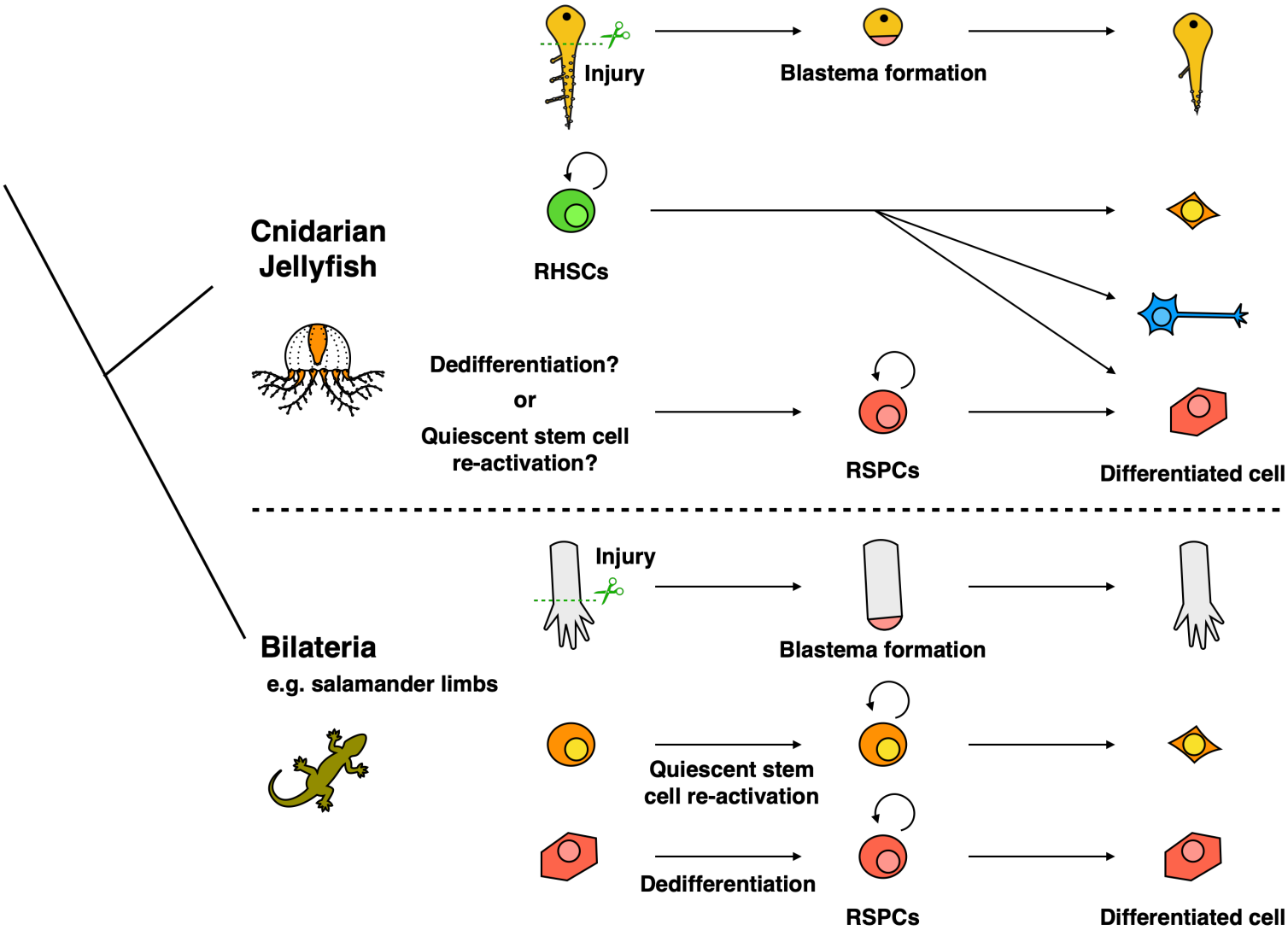
B Appendage regeneration evolution model